

# **Navicular Bone Location in Radiographs and Solar Scintigrams**

*The radiographic location of the equine navicular bone in  
the front legs, the effect of leg positioning, and a method to  
position a navicular bone region of interest in a solar  
scintigram*

Charles Ley

Division of Diagnostic Imaging and Clinical Pathology  
Department of Biomedical Sciences and Veterinary Public Health  
Faculty of Veterinary Medicine and Animal Science

**Swedish University of Agricultural Sciences  
Uppsala 2006**

The present thesis is a partial fulfilment of the requirements for a Master of Science Degree in Veterinary Medicine for International Students at the Swedish University of Agricultural Sciences (SLU), in the field of Diagnostic Imaging

Charles Ley,  
Division of Diagnostic Imaging and Clinical Pathology  
Department of Biomedical Sciences and Veterinary Public Health  
Faculty of Veterinary Medicine and Animal Science  
Swedish University of Agricultural Sciences (SLU)  
P.O. Box 7029, SE- 750 07 Uppsala, Sweden  
Print: SLU Service/Repro, Uppsala 2006

The goal is to produce a useable image, not a perfect one.  
John W Hirshfeld 2003.

To Cecilia, Timothy and Kristoffer

## **Abbreviations used in this thesis**

$^{99m}\text{Tc}$  – Technetium- 99m  
AR- conventional analogue radiology  
CR- computed radiology  
DR- digital radiology  
PACS - picture archiving communication system  
IRU- increase in radiopharmaceutical uptake  
kVp- kilovoltage peak  
LEAP - low energy all purpose (collimator)  
LM - lateral to medial projection  
mAs- milliamperere-seconds  
MBq- megabecquerel  
PIPJ – proximal interphalangeal joint  
PrDi – proximal to distal projection  
ROI- region of interest  
RU- radiopharmaceutical uptake

# Contents

<b>Abstract</b>	6
<b>Introduction</b>	7
<b>Aims of the Investigations</b>	10
<b>STUDY OF LITERATURE</b>	
<b>Anatomical detail of a skeletal image</b>	
Spatial resolution	10
Signal and noise	11
Contrast	11
<b>Radiology</b>	
Making a radiograph	12
Spatial resolution of radiographs	13
Contrast and density resolution of radiographs	15
<b>Scintigraphy</b>	
Making a bone phase scintigram	17
Spatial resolution of scintigrams	18
Contrast and density resolution of scintigrams	23
<b>The navicular bone</b>	
Navicular disease	24
Navicular disease and scintigraphy	24
The solar projection scintigram	25
Superimposition of other body regions on the navicular region	25
Count acquisition for the solar scintigram	25
Evaluation of the solar scintigram	26
Positioning of the navicular region of interest	26
<b>References</b>	27
<b>RESEARCH REPORT</b>	
Introduction	29
Materials and methods	31
Results	41
Discussion	43
Conclusion	46
References	46
<b>ACKNOWLEDGEMENTS</b>	48

## **Abstract**

Ley, CJ. 2006. Navicular bone location in radiographs and solar scintigrams.

The radiographic location of the equine navicular bone in the front legs, the effect of leg positioning, and a method to position a navicular bone region of interest in a solar scintigram.

Masters thesis. ISSN 1403-2201. Report number 55.

The anatomical location of the navicular bone region in the solar projection scintigram has not been clearly established and it is often not possible to define the navicular bone in solar projection bone phase scintigrams. This is due to the relatively poor anatomical detail of scintigrams. In contrast, skeletal radiology has high spatial and contrast resolutions and skeletal structures can be well defined, however radiology does not provide the functional information that scintigraphy does.

Techniques using quantitative analysis of scintigrams, particularly the navicular bone region in the solar scintigram, seem to be becoming more popular. For these techniques to be reliable, correct positioning of regions of interest or profiles is essential, and this requires accurate location of anatomical structures. Superimposition of the proximal interphalangeal joint region on the navicular bone region in the solar projection scintigram is a recognised problem when evaluating the palmar regions of the foot for abnormal areas of radiopharmaceutical uptake, and this superimposition could result in incorrect interpretation of the radiopharmaceutical uptake in a navicular bone region of interest.

It was hypothesised that landmarks in the solar projection scintigram could be used to locate the navicular bone region and that there would be the least superimposition of the proximal interphalangeal joint region on the navicular bone region when the interphalangeal joints were flexed.

Measurements were taken from radiographs of specimen horse legs to determine if the navicular bone moved relative to the distal phalanx when the leg position was changed. Using both specimen horse legs and live horses radiographs were examined to investigate the navicular bone position relative to landmarks on the distal phalanx. Radiographs of specimen horse legs were taken with the legs positioned in maximum interphalangeal joint flexion, maximum interphalangeal joint extension and a fixed angle (50°), and the degree of overlap of the proximal interphalangeal joint region and the navicular bone region was measured.

Leg positioning did not change the position of the navicular bone relative to the distal phalanx in a dorsal to palmar plane. Very little variation existed between individuals in: the ratio of the distance from the dorsodistal margin of the distal phalanx to the dorsal margin of the navicular bone (P3-Navicular) compared to the dorsopalmar length of the navicular bone (Navicular length), the ratio between the maximum lateral width (P3 width) of the distal phalanx and P3-Navicular, and the ratio between P3 width and the maximum lateral width of the navicular bone (Navicular width). In contrast, large variation existed in the ratio of the distance from the palmar aspect of the palmar processes to the palmar aspect of the navicular bone (Navicular-PP), compared to Navicular length.

Positioning the pastern in maximum flexion resulted in the least overlap of the proximal interphalangeal joint and navicular regions. It is recommended that the phalanges are flexed and the sole is placed flat on a raised horizontal gamma camera when the solar projection is acquired.

The measurement ratios of the distal phalanx and the navicular bone were applied to a solar projection scintigram to predict navicular bone position and position a navicular bone region of interest using anatomical landmarks that could be distinctly identified in the scintigram.

Key words: horse, equine, solar projection, scintigraphy, radiology, navicular, distal sesamoid bone, foot, proximal interphalangeal joint, pastern.

## Introduction

Radiology and scintigraphy are diagnostic imaging techniques that are commonly used to investigate the cause of equine lameness. The two techniques provide different, but complementary information about the equine skeleton and the results of the techniques are often used together to make a diagnosis.<sup>1</sup>

Navicular disease is a common cause of equine lameness and the value of scintigraphy in the diagnosis of this problem is well described.<sup>2-13</sup> The solar scintigram is reported to be the most sensitive projection for detecting navicular disease.<sup>2</sup>

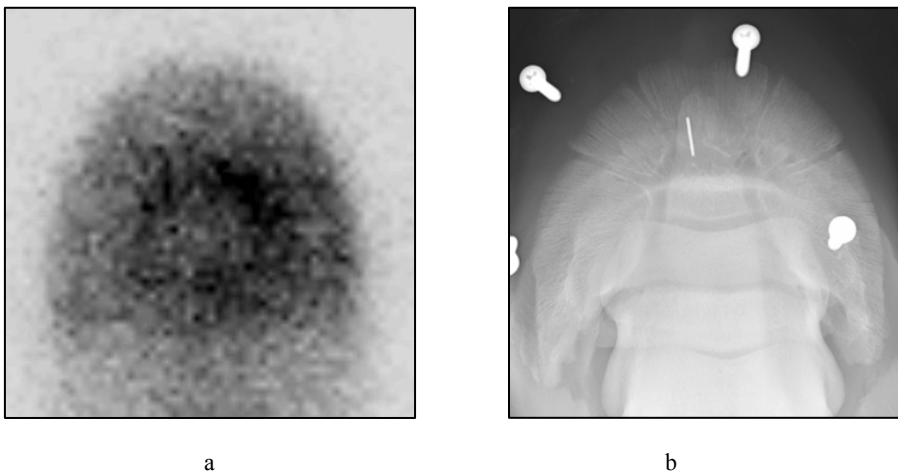


Figure 1. (a) A solar projection scintigram. (b) A proximodistal projection radiograph of the foot.

The solar projection scintigram and a proximodistal projection radiograph both image the same area of the horse at the same angle of projection (Figures 1a and 1b). The solar scintigram is taken by placing the horses' foot flat on a protective surface, on the surface of the gamma camera collimator. The solar scintigram is orientated as though the viewer is looking up through the sole of the horses' foot (Figure 2a). A proximodistal radiograph is taken with the sole of the horses' foot flat on an x-ray cassette and the x-ray beam perpendicular to the cassette and centred on the middle of the foot (Figure 2b).

Radiology provides morphological information, whereas scintigraphy provides primarily functional metabolic information.<sup>1,12</sup> Due to the different way that radiographs and scintigrams are produced, there is higher anatomical detail in the radiographs compared to the scintigrams. The amount of anatomical detail in a radiograph or scintigram is dependant on spatial resolution, density resolution, dynamic range, and the signal to noise ratio.<sup>14</sup>

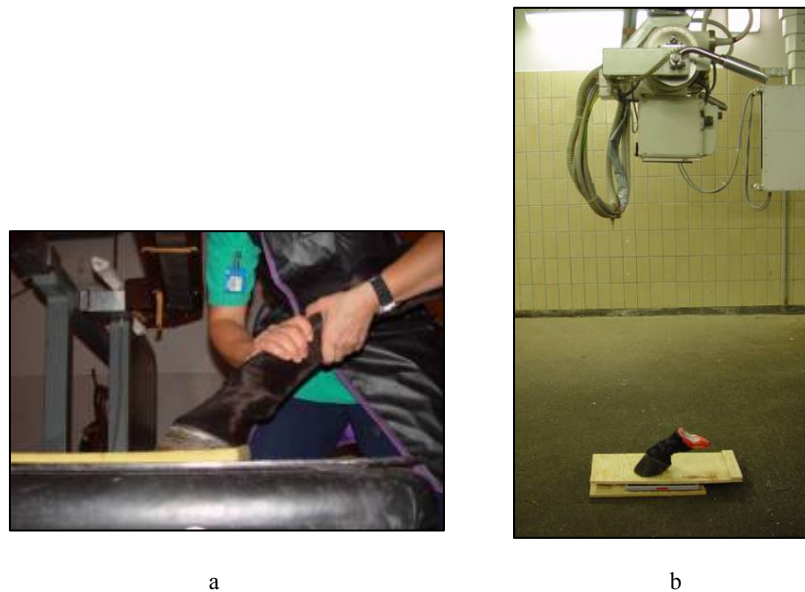


Figure 2. (a) The positioning for a solar projection scintigram of a live horse. (b) The positioning for a proximodistal projection radiograph of the foot of a specimen.

In bone phase scintigrams, the image that is produced shows the margins of the skeleton as indistinct borders, smoothing and colour displays can be used to make these borders more distinct. There are specific areas of the skeleton in a scintigram that normally have relatively higher radiopharmaceutical uptake (RU) and other areas with relatively low RU. This means that some regions of the skeleton are reliably and repeatedly detectable in a scintigram and these regions can be used as landmarks to identify other less obvious regions.

In the solar scintigram, portions of the distal phalanx and middle phalanx are always superimposed on the navicular bone region. The navicular bone normally appears as a small and low intensity structure and it is often not possible to define the navicular bone in solar scintigrams. For this reason, other anatomical structures are commonly used as landmarks to estimate the position of the navicular bone. Various techniques have been used to localise the navicular region in solar scintigrams, these include; superimposing radiographs<sup>2</sup>, using anatomical landmarks<sup>7</sup>, and by using observations from previous clinical cases.<sup>8</sup> The accuracy of these techniques in identifying the navicular bone region has not been investigated. Once the navicular region is localised a region of interest (ROI) can be drawn around the navicular region.

Scintigrams can be examined subjectively or quantitatively. Subjective examination requires the viewer to compare patterns in the image being examined with memorised expected patterns of a normal individual. For this type of examination to be accurate, it requires that the viewer have considerable prior experience with normal and abnormal images. This technique should result in the entire image being evaluated. Quantitative examination uses regions of interest



(ROIs) or profiles that are placed manually, semi-automatically, or automatically on the scintigram.<sup>15</sup> The data in these specific regions of the scintigram is then used to calculate statistics or plot graphs. This information can then be used to compare specific areas, and when using ROIs this is usually expressed as a ratio. The ratio can be compared to the assumed normal contralateral limb, or a normal range of values. Since navicular disease is often bilateral, it is generally not possible to use the contralateral leg as a 'normal control', thus a normal range is required. The accuracy of the anatomical localisation is especially important when quantitative techniques are used since, the ROIs or profiles must be placed in the correct anatomical position for the ratios to be correct. If accurate ranges for these ratios are to be developed, it must be possible to accurately and repeatedly identify the required skeletal region in all individuals examined.

Equine bone phase scintigrams are usually examined subjectively before they are examined quantitatively, and the quantitative information is often used to support or refute a subjective impression. If accurate normal values of the ratios of two areas are available, this might improve diagnostic accuracy, especially in less experienced observers.

A variable amount of superimposition of the proximal interphalangeal joint region and the metacarpophalangeal joint region on the navicular region is present in the solar projection scintigram.<sup>2,11</sup> This can result in both false positive<sup>2</sup> and probably false negative diagnoses of abnormalities in the navicular region. The amount of superimposition of these joint regions on the navicular region has not previously been reported.

This study focused on identifying the navicular region in solar scintigrams using the superior anatomical detail of radiographs. A series of ratios of length and width of skeletal structures were identified in the radiographs. The ratios were used on a solar scintigram to predict the position of the navicular bone region in the scintigram and place a region of interest over it. The study also investigated the overlap of the proximal interphalangeal joint region on navicular region in different pastern angles, again using radiographs.

## **Aims of the Investigations**

The aims of this study were to identify a technique that would result in accurate placement of a navicular bone region of interest, and describe a positioning technique that minimises superimposition of the proximal interphalangeal joint region on the navicular bone region in solar scintigrams.

## **STUDY OF LITERATURE**

### **Anatomical detail of a skeletal image**

Anatomical detail refers to the ability to define separate anatomical (in this case skeletal) structures in an image. It is determined by the spatial resolution, contrast resolution, and the signal to noise ratio. The anatomical detail of a radiograph is much higher than that of a scintigram (compare Fig 1a to Fig 1b).

#### **Spatial resolution**

The spatial resolution is the ability to define two separate small point sources in an image, and can be defined in millimetres. The spatial resolution is influenced by both imaging equipment and patient factors.

The modulation transfer function is a technique that can be used to measure the spatial resolution of an imaging system.<sup>16,17</sup> This technique quantifies the ability of a system to depict spatial frequencies (pairs of lines/cm) and the modulation transfer function is calculated as an index between the input (ideal image) and the output (actual image) of the imaging system. An ideal imaging system would have a modulation transfer function of one.

The spatial resolution of analogue imaging techniques is strongly influenced by the type of film used.

Digital images are composed of small squares, arranged in rows and columns called picture elements or pixels. The size or matrix of a digital image is described by how many pixels that are present along the X-axis and the Y-axis. If an image is composed of pixels that are too large, it will have a mosaic or checkerboard appearance (Figure 3). When the image pixels are smaller than the computer screen pixels, the computer screen matrix will determine the spatial resolution of the image. Images with very small pixels allow digital zooming without loss of spatial resolution. A mosaic like image will also develop if the pixels in the zoomed image are enlarged so much that they become bigger than the pixels of the computer screen. Images with small pixels have high spatial resolution.



Figure 3. A scintigram with large pixels (matrix 64 x 64), which has a mosaic or checkerboard appearance.

### **Signal and noise**

The signal is the information in the image that is due to actual differences in the imaged object. Noise is the variation in the information in the image that is not due to the patient. Noise degrades the diagnostic image, by both adding to and subtracting from the signal. The signal to noise ratio is a measurement that can be used to compare image quality. Images with a high signal to noise ratio per pixel have the best anatomical detail.

### **Contrast**

In radiology, contrast is defined as the difference in film blackness between areas in a radiograph<sup>18</sup>, and it is a term widely used in conventional analogue radiology. The scale of contrast, also called the grey scale or latitude, is the range of shades of grey in a radiograph<sup>18</sup>. These terms can create confusion, since an image with high contrast has a low scale of contrast, and visa versa.

In digital imaging the terms density resolution, dynamic range and contrast resolution are more commonly used to describe the contrast characteristics of an image.<sup>14,16</sup>

The density resolution (also called the image depth) in an image is the ability of a computer screen or film to display separate shades of grey or colour in the image. In digital images, it is determined by number of bits of data or number of counts that can be stored in each pixel.<sup>14-16</sup> In radiology and scintigraphy, the shade of grey or colour of each pixel is determined by how many photons have been received in the area of each pixel.<sup>15</sup>

Dynamic range is the ratio of the brightest to the darkest region of the image.

Contrast resolution is defined as the ability to see low-contrast objects in an image.<sup>14</sup> Contrast resolution combines contrast and scale of contrast, but is also strongly influenced by the signal to noise ratio. As noise levels decrease or signal increases, the contrast of the object becomes more perceptible.<sup>14</sup>

It is important to note that even though an image maybe in a format that has high density resolution, it is still possible to obtain an image with a low dynamic range

due to the exposure/acquisition settings and post processing of the image. Such an image would then have a low density resolution. An image that has a low density resolution (due to the exposure/acquisition settings, post processing or monitor) will appear to have contours of greyness or colour<sup>16</sup>.

## **Radiology**

### **Making a radiograph**

Radiology is a transmission imaging technique performed by directing a beam of x-ray photons through a body part. The energy of the x-ray photons is determined by the kilovoltage peak (kVp) and the amount of x-ray photons in an exposure is determined by the milliamperere-seconds (mAs). The x-ray photons are detected by an imaging plate or film, which is placed on the opposite side of the body part from where the x-ray photons entered. The absorption of the x-ray photons by the body varies according to density and thickness of the body part and the components that make up the body part (soft tissues, fluid, bone, fat and gas). Changes that can be detected in radiographs include changes in shape, position, size, number, opacity, and margination.<sup>18</sup>

Increasingly radiology is becoming computerised. Currently there are three possible methods for recording radiographs. These are conventional analogue radiology (AR), computed radiology (CR), and digital radiology (DR). All three systems use the same x-ray tube to produce the x-ray photons that create the radiograph, but all three systems convert the incident x-ray photons into a radiographic image in different ways.

#### *Conventional Analogue Radiology*

The image is created in conventional films by x-ray photons striking the phosphorescent crystals in the intensifying screen, which results in the release of flashes of light. These flashes plus the remaining x-ray photons causes reduction of silver halide crystals in the film to silver in the emulsion adjacent the place where the x-ray photon entered the cassette. The reduced crystals are called latent image centres. The film is then immersed in a developer and the silver halide crystals are reduced to silver in the regions immediately surrounding the latent image centres. Finally, the film is placed in a fixer, which removes any unexposed silver halide crystals from the film before the film is washed. This results in an analogue image on radiographic film.<sup>14</sup>

### *Computed Radiology*

Computed radiology (CR) uses a cassette that looks just like a conventional analogue cassette, but instead of film, the cassette contains an imaging plate. The active component of the imaging plate is photostimulatable phosphor (barium fluorohalide compound crystals and bivalent europium ions), which invokes photostimulated luminescence. Photostimulated luminescence is the initial step in creating the radiographic image. It occurs when information about the primary excitation (the x-ray photons reaching the imaging plate) is recorded/remembered in the phosphor substance that is the active component of the imaging plate. This information can be retrieved by doing a second excitation (Laser scanning) of the imaging plate. The luminescence from the imaging plate during the second excitation is converted to electric signals by photomultiplier tubes and recorded in digital format on a computer. The residual image is then removed from the imaging plate by a bright light so the imaging plate can be reused.<sup>16</sup>

The matrix of the CR image is selected in the imaging plate reader. The actual pixel size in the CR image can be selected automatically or manually in the image plate reader depending on the desired spatial resolution and the size of the image plate<sup>16</sup>.

### *Digital Radiology*

In digital radiology (DR), the image receiving plate is called a detector. The detector communicates directly with a computer system via an electric cable, without the use of an imaging plate. When the x-rays reach the detector, they are absorbed by a scintillator, which converts the x-ray photons into visible light. The light is converted into digital electrical signals by sensor cells and these signals become the radiographic image that is displayed on a computer screen. The DR detector has a fixed matrix depending on the size and number of the sensor cells.

### *Picture archiving communication system*

After the CR or DR radiograph is made and judged of acceptable quality, the image is usually sent to a picture archiving communication system (PACS) where the images are analysed and digitally manipulated. A function that was used extensively in this study was the distance and angle measurement function in the PACS.

In this study, a Fuji CR system (Fujifilm FCR XG-1. Fuji Medical Imaging Co.Ltd.Japan) and a General Electric PACS (Centricity RA 600 V6.1 Diagnostik, General Electric Medical Systems, Slough, UK.) were used.

## **Spatial resolution of radiographs**

Radiographs, particularly when made of extremities have high spatial resolution when the appropriate equipment is used. The smallest objects that can be defined in radiographs taken in a typical clinical situation are; 0.08mm in AR and 0.17mm in DR.<sup>14</sup> The spatial resolution in a radiograph is influenced by; the patient positioning, the body region being examined, exposure settings, the x-ray tube, the grid, the screen (in the conventional analogue film system), the film/imaging plate and processing.

### *Motion*

Motion during exposure of a radiograph results in blurring and it is one of the most common causes of reduced spatial resolution. The effects of motion can be reduced by ensuring the x-ray tube does not move during the exposure, ensuring the patient does not move during exposure (restraint, sedation, or anaesthesia), and using the shortest possible exposure time.<sup>18</sup>

### *Penumbra*

The term penumbra means edge unsharpness. A large penumbra results from increased divergence of the primary x-ray beam and causes reduced spatial resolution. A large penumbra occurs when; the focal spot of the x-ray tube is large, the focal spot to imaging plate distance is short, and when the patient to imaging plate distance is large.<sup>18</sup>

### *Scatter*

Radiation that is scattered in the tissues and reaches the x-ray film will also reduce spatial resolution. This becomes a significant problem when thicker body parts (more than 10cm thick) are radiographed. When x-ray photons interact with body tissues they can undergo Compton scattering, the photoelectric effect, and coherent scattering.<sup>18</sup>

Compton scattering occurs when an x-ray photon ejects an outer shell electron from a tissue atom, and is scattered (called a Compton photon) in a random direction. The Compton photon has lower energy than the original x-ray photon, but still has enough energy to pass through tissue and expose the film or imaging plate. Such an exposure is called film fog since it represents noise and not signal, and causes a foggy appearance on radiographic film.<sup>18</sup>

The photoelectric effect occurs when an x-ray photon ejects an inner shell electron from a tissue atom. This results in absorption of the x-ray photon by the atom and release of characteristic radiation. This radiation is low energy. It is absorbed by the surrounding tissue and does not result in film fogging.<sup>18</sup>

Coherent scattering occurs when an x-ray photon interacts with an object and changes its direction. There is neither absorption nor change of energy of the photon. The percentage of x-ray that undergo coherent scattering is small, approximately 5%. The scattered radiation has the same energy as the original x-ray photon, and causes film fogging.<sup>18</sup>

Film fogging caused by scatter can be partially overcome by using a grid formed of thin parallel lead strips. The grid absorbs oblique, scattered radiation but allows parallel diagnostically useful x-ray photons to pass through.

### *Screens*

Fine detail screens are used in AR to maximise the spatial resolution but still allow a low mAs value so irradiation of the patient is minimised. These screens have smaller crystals than regular screens so that the crystal exposes a smaller region on the x-ray film, thus smaller structures can be defined. The maximum spatial resolution that can be obtained in AR is when the x-ray film is used without

screens, for example in dental non-screen film. This technique results in very high mAs exposure values, resulting in a higher radiation dose to the patient and possible problems with motion artefact.

### *Film/imaging plate/detector*

Various types of film are available for AR. The films that give the best spatial resolution are the fine detail and single emulsion films. These films have smaller crystals in thinner layers, which results in the each x-ray photon exposing a smaller region of the film when compared to fast films. The exposure times for these films are long because more x-ray photons are required to expose the film.

In CR, the photostimulable phosphor in the imaging plate functions in a similar way to the conventional screen film combination. Thus, it is possible to vary the composition of the photostimulable phosphor and change the characteristics of the imaging plate. New CR imaging plates are being developed that have higher spatial resolution.<sup>16</sup>

CR and DR produce digital images that are viewed on a computer screen. The pixel size in the original image is a very important factor in the spatial resolution of the image. The pixel size in CR is usually selected automatically in the imaging plate reader depending on which size of cassette is being used, and the body part being examined.<sup>16</sup> The detector in DR has a fixed pixel size. This means when small regions are radiographed using a large detector the digital zooming must be used to make the image a suitable size. Digital zooming can result in lower spatial resolution.

The computer screen that is used to view the digital images is one of the most important factors in determining the anatomical detail of CR and DR images. An image that is better than the screen it is viewed on is of little use, except when digital zooming is used. The important factors are the pixel size, the dynamic range, and the screen luminance. High-resolution screens (in the range of 2048 x 2560 pixels), which may be cathode ray tube or liquid crystal display monitors, are used commonly for diagnostic radiology. For radiology, the black and white screens are superior to the colour screens since they have a higher dynamic range.<sup>19</sup>

## **Contrast and density resolution in radiology**

When radiographs of the skeleton are taken correctly, they have high contrast resolution, high density resolution, and high dynamic range. This is due to the large difference between the absorption of x-ray photons in the calcium containing bone compared to soft tissue and fat.<sup>4</sup>

Factors important in the quality of contrast in a radiograph include; exposure settings and dynamic range of the image receiving system, subject contrast, film/imaging plate/detector contrast and scatter.

### *Dynamic range*

When using AR it is vital that the exposure settings are correct, since over or under exposed radiographs have a low dynamic range and therefore low density resolution. CR and DR allow for a relatively large variation in the exposure

settings. The reason for the difference is the variation in the dynamic range between the analogue and the digital systems. This can be displayed as a characteristic or Hunter and Driffield curve (Figure 4). For conventional analogue film, this curve is a sigmoid shape. The straight central segment of this curve is the region where the images have the highest dynamic range; the curved marginal areas have low dynamic range. CR and DR have a linear dynamic range and as long as the image is not at the very top or bottom of the graph then dynamic range should remain constant.

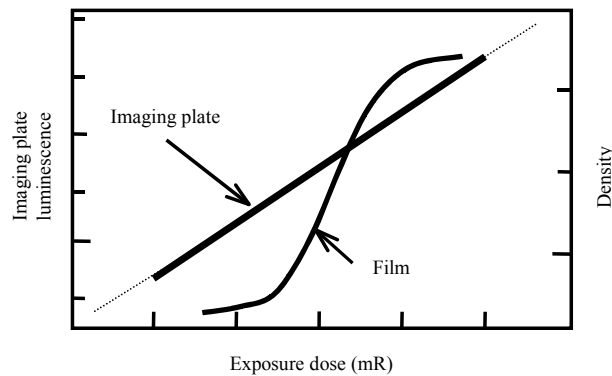


Figure 4. Characteristic curve showing the dynamic range of an imaging plate and x-ray film relative to the exposure dose.

### *Subject contrast*

Subject contrast refers to the contrast of the body region being radiographed. The attenuation of x-ray photons varies according to tissue thickness, physical density differences, and atomic number differences. Since these factors vary in different body regions, the contrast in radiographs from different body regions varies.

The variation in exposure settings also allows for radiographs of different contrast to be taken. Settings with low kVp and high mAs result in high contrast images with a short grey scale, whereas high kVp and low mAs settings result in low contrast images with a long grey scale. The reason for this effect is that lower energy x-ray photons (low kVp) have low penetration of thick, dense, high atomic number tissues, but still pass through thin, less dense tissues, but high energy x-ray photons (high kVp) more easily pass through all tissues. Thus, there is a larger difference between the numbers of x-ray photons passing through different types of tissue with low kVp (the image tends to be black and white) than there is with high kVp (the image has more shades of grey).<sup>18</sup>

The effects of subject contrast are less in CR and DR due to the possibility to post-process images and the possibility to make large changes to the contrast and grey scale of the pixels in the image. The important factor is that the amount of x-ray photons (signal) reaching the imaging plate are enough to achieve a satisfactory signal to noise ratio.<sup>16</sup> Using higher kVp values will result in penetration of thick, dense high atomic weight regions. These regions might otherwise absorb all the x-ray photons and not be possible to image. If kVp values



are too high when radiographing a small body part, the amount of x-ray photons absorbed by the body may be too low to create an image (the image would be black).

#### *Film/imaging plate/detector contrast*

Film contrast is influenced by the type and size of the silver halide grains in the film emulsion. Both high-contrast and latitude (low contrast) films are available. In a digital image, contrast is influenced by the type of plate reader or detector, the density resolution and dynamic range of the image and the screen.

#### *Scatter*

This is discussed in the spatial resolution section. The same principles apply to contrast and density resolution.

#### *Artefacts*

There are a series of artefacts including prior exposure of an x-ray film to light, and using an imaging plate that has not been processed for a few months, which will result in fogging of the image and reduced contrast.<sup>16</sup>

## **Scintigraphy**

### **Making a bone phase scintigram**

Scintigraphy is a diagnostic imaging technique where a radiopharmaceutical is given and taken up by a body system (determined by the marker). The radiation emitted from the body is detected by a gamma camera and displayed as an image or as data. Equine bone phase scintigraphy is one of the most common forms of scintigraphy in veterinary medicine.<sup>20</sup> To perform bone phase scintigraphy sodium technetium-99m pertechnetate ( $\text{Na}^{99\text{m}}\text{TcO}_4$ ) is mixed in a radiopharmaceutical kit with a diphosphate. Methylene diphosphate (MDP) and hydroxymethane/hydroxymethylene diphosphonate (HDP/HMDP) are common bone seeking pharmaceuticals. The freshly mixed radiopharmaceutical is injected intravenously (recommended dosages vary from 11.4-18.5 MBq/kg).<sup>3,20</sup> The majority of the skeletal uptake of the radiopharmaceutical occurs in the first 20-30 minutes after injection, but the radiopharmaceutical does not clear from the soft tissues for 1-2 hours. The half-life of  $^{99\text{m}}\text{Tc}$  is six hours.<sup>20</sup> The bone phase images are acquired approximately two hours after the injection of the radiopharmaceutical, at the time when the radioactivity of the  $^{99\text{m}}\text{Tc}$  is still high, and when the ratio between the skeletal radioactivity compared to the soft tissue radioactivity is the highest. The scintigrams are acquired using a gamma camera, and images are viewed on a computer using nuclear medicine software.<sup>3,11,12,20,21</sup>

Bone phase scintigraphy primarily gives functional information on the metabolism of the skeleton. It is used to identify areas in the skeleton where there is increased osteoblast activity, which may occur in response to traumatic injury, inflammation, infection, or neoplasia of the skeleton. The radiopharmaceutical binds preferentially to areas increased metabolism so these areas appear with the

colour or shade of grey representing the highest counts. Areas in a scintigram that have an abnormal increase in the count intensity are called areas of increased radiopharmaceutical uptake (IRU).<sup>3,11,12,20,21</sup>

### **Spatial resolution of scintigrams**

The spatial resolution of a scintigram is influenced by the gamma camera and collimator, patient factors and computer processing factors.

#### *The gamma camera and collimator*

The gamma camera and collimator are usually the limiting factors in the spatial resolution of a scintigram. The intrinsic spatial resolution at the face of the sodium iodide crystal of the gamma camera is normally between 1-2mm.<sup>22</sup>

The function of the collimator is to filter the cloud of  $\gamma$ -photons that are being emitted in all directions by the patient so that only photons passing perpendicular to the camera face reach the camera crystal. This allows the computer to estimate the origin of the photons and build up an image of the radiation emitted by the patient.<sup>22</sup> The most commonly used collimator for skeletal scintigraphy is a low energy all purpose (LEAP) collimator. This is a parallel-hole-collimator, which has multiple identically shaped round or hexagonal openings, which are perpendicular to the detector surface of the gamma camera. The septa between the holes in the collimator are usually made of lead.<sup>23</sup> The LEAP collimator has mid-range resolution and sensitivity. A typical spatial resolution for a LEAP collimator is about 4-5mm at the collimator surface.<sup>22</sup> A high-resolution collimator that has deeper and smaller holes, typically has a spatial resolution of about 2-3mm.<sup>22</sup> High resolution collimators are rarely used in skeletal scintigraphy since they result in excessively long acquisition times.

#### *Pulse height analyser*

The pulse height analyser is an energy discriminator that limits the recorded signal to a specific amplitude signal range that is called the energy window. The energy window is centred on the energy peak of the radioisotope and the window is usually set at 10% either side of this peak. Since scattered photons have lower energy than incident photons the pulse height analyser excludes many of the from the scintigram image. This improves spatial resolution.<sup>22</sup>

#### *Distance*

It is important that the body region being examined is as close to the gamma camera as possible when the scintigram is acquired. As the distance between the gamma camera and the body region increases, more photons that are not parallel to the collimator holes are able to pass through the collimator. The non-parallel photons will be recorded on the scintigram in a position that does not reflect their true origin. The result is a blurred scintigram that has reduced spatial resolution.<sup>24</sup> A LEAP collimator with a spatial resolution of 4-5mm at the collimator surface has a spatial resolution of 9-10mm for an object that is 10cm from the collimator surface.<sup>22</sup>

Distance is particularly a problem when imaging areas covered with thick soft tissue, since the area of interest will often be a significant distance from the camera crystal.

However, small changes in the body part to gamma camera distance should not change the amount or intensity of the radiopharmaceutical uptake detected from the body part. This is because as the distance increases the percentage of photons that get through the collimator increases (as mentioned above they become more parallel) in a similar proportion to the decrease in photons due to the inverse square law.<sup>24</sup>

### *Dose and time*

The amount of radiation (counts) received by the gamma camera from the patient (the signal) during the acquisition of an image is determined by the acquisition time and the amount of radiation emitted per second by the patient.<sup>25</sup> Long acquisition times and patients that emit high amounts of radiation per second generally result in images with higher spatial resolution (Figure 5).

The amount of radiation emitted by the patient is determined by the dose of radiopharmaceutical given intravenously, the age of the patient, the blood flow to the region being examined, and the level of metabolism in the skeletal structures in the region being examined.<sup>25</sup> High doses of radiopharmaceutical result in high-count rates per second. Young animals take up more radiopharmaceutical in their skeletons, thus emitting more gamma radiation than older animals.<sup>25</sup> In horses low blood flow especially to the distal limbs can result in poor uptake of the radiopharmaceutical by the skeleton.<sup>26</sup> Long acquisition times can result in problems with motion blur.

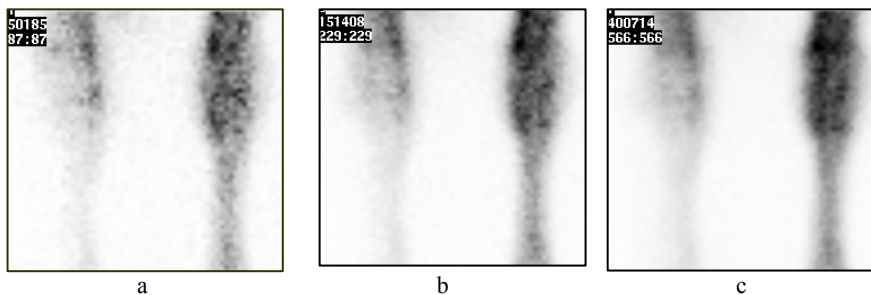


Figure 5. Static images made by adding dynamic frames of a dorsal image of both carpal joints. (a) A scintigram with a low number of total counts (50185), the spatial resolution, and contrast resolution are poor and the image is noisy. (b) A scintigram with a moderate number of total counts (151408), spatial resolution, and contrast resolution are better than (a) but not as good as (c). (c) A scintigram with a high number of total counts (400714), this image has the best spatial resolution and contrast resolution and the signal to noise ratio is good.

### *Movement*

Spatial resolution of the scintigram can be severely reduced by movement of the patient during scintigram acquisition. Movement is a constant possibility during acquisition in equine scintigraphy, since most horses are examined standing and under sedation. Bone phase images of the distal limb are usually taken using static acquisition, that is, a single scintigram image is built up from all the photons received by the gamma camera during the acquisition time. If the body region being examined moves during the acquisition time, there will be blurring of the scintigram and reduced spatial resolution. This problem can be partially overcome by using dynamic acquisitions and motion correction software (Figure 6).

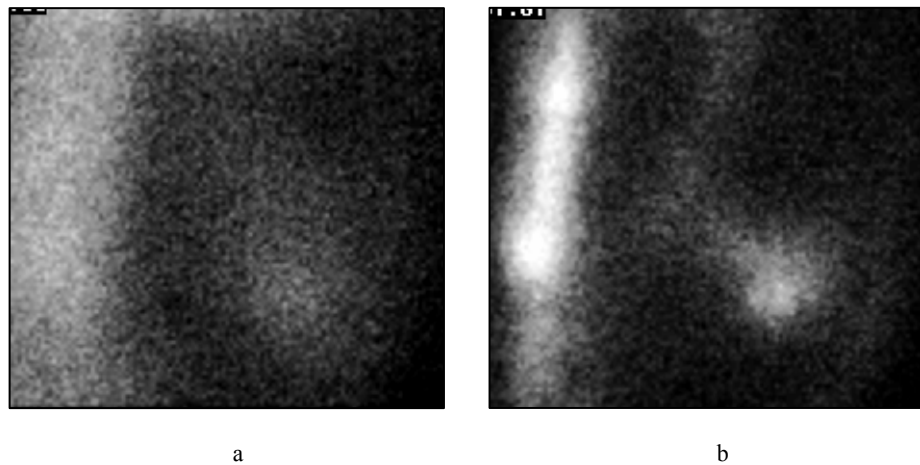


Figure 6. Scintigrams of the right coxofemoral joint region of a horse that was swaying during image acquisition, (a) before motion correction, (b) after motion correction.

### *Matrix*

Matrix refers to the number of pixels in the grid that makes up a digital image on a computer screen. A matrix of 256 x 256 means that there are 256 pixels across the top and 256 pixels down the side of the image, thus 65 536 pixels make up the image. For a standard 40cm field of view camera, a 128 x 128 matrix has 3.1mm<sup>2</sup> sized pixels, and a 256 x 256 matrix has 1.56 mm<sup>2</sup> sized pixels.<sup>27</sup>

The matrix is selected before the scan, according to which area is examined and the number of counts obtained from the area. The largest matrix (usually 256 x 256 in equine bone phase scintigraphy) results in the image that contains the smallest pixels and highest number of pixels per image, and in some cases the highest spatial resolution. Images of small structures with relatively high counts per pixel are suitable for a large matrix, and images of larger structures with a larger spread of counts (less counts per pixel) should have a lower matrix. The lower matrix settings (128 x 128 and 64 x 64) have larger and a lower number of pixels and often a lower spatial resolution.<sup>15,22</sup>

It would be expected that selecting the highest matrix would give the images with highest spatial resolution. This is not true, since the spatial resolution is already limited by the camera and collimator (4-5mm using a LEAP collimator

with the body part very close to the surface of the collimator) and selecting a matrix with pixels smaller than the possible spatial resolution of the collimator has no advantage. The other disadvantage of high matrix images is that the result in a low number of counts per pixel and this causes problems with noise (see below).

The matrix of an image can be changed after the image has been made. Increasing the matrix of a completed image results in more and smaller pixels in the image but the image will remain identical (Figure 7). Decreasing the matrix of a completed image will result in less and larger pixels in the image. Each large pixel will have a value, which is the mean of the smaller pixels that have been combined to make the large pixel.<sup>15</sup> This results in an image with less spatial resolution but also less noise, and there will be a variable change in contrast resolution the depending on the number of counts in the image (Figure 7). For these reasons, as long as plenty of computer memory is available, it is always better to select the highest reasonable matrix when acquiring an image. The matrix can always be decreased later, but it cannot be usefully increased.

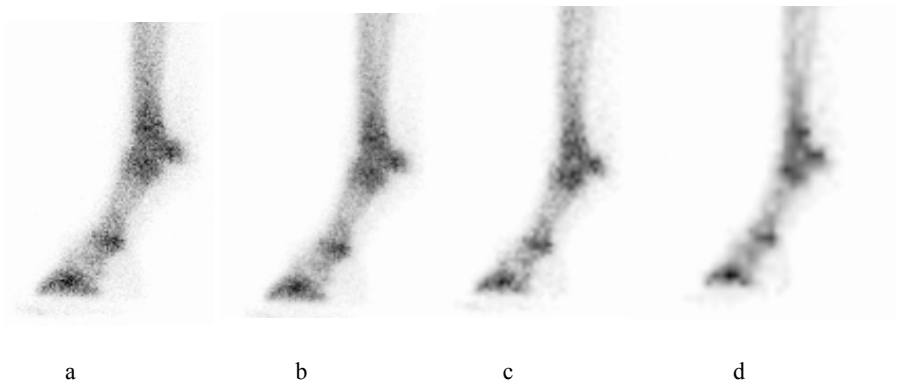


Figure 7. A scintigram of the left front foot with different matrix settings. The original image (a) was acquired with a matrix of 256 x 256, and this image is noisy but has good spatial resolution. The matrix of image (a) was changed to 512 x 512 resulting in image (b), which appears identical to image (a). The matrix of image (a) was changed to 128 x 128 resulting in image (c), this image has less noise, good spatial resolution and contrast resolution, and is probably the best matrix setting for this image. The matrix of image (a) was changed to 64 x 64 resulting in image (d), this image is starting to get a mosaic appearance, the spatial resolution is poor, but the contrast resolution is still good.

### *Signal and noise*

The ratio of signal to noise in a scintigram is an important factor in the spatial resolution. Sources of noise in a scintigram include; Compton scatter, inherent noise in the camera system and Poisson noise.<sup>27</sup>

The principle of Compton scatter is the same in scintigraphy as it is in radiology, except that in scintigraphy the significant Compton scatter is occurring in the sodium iodide crystal of the gamma camera.<sup>22</sup> The noise from Compton scatter is minimised by using the pulse height analyser.

Poisson noise is due to the random nature of radioactive decay. A radionuclide emits an average number of photons per second, but the exact timing and the direction of each photon are random. This random timing and direction of the

photons means that even when there is a uniform field source of a radionuclide the number of photons counted in each pixel is not the same, but the distribution of the number of counts in each pixel follows a Poisson distribution.<sup>14</sup> Because decay follows a Poisson distribution it is known from statistics that the standard deviation of the counts, which is equal to the image noise, can be calculated from the mean number of counts per pixel in a region or image (Equation 1).<sup>14</sup> The relative noise can also be calculated from the value of the mean number of counts per pixel in a region or image (Equation 2).<sup>14</sup> From this equation for relative noise, it can be seen that if the mean number of counts per pixel is low then the relative amount of image noise will be high, and visa versa (Figure 5).<sup>14</sup> The signal to noise ratio is the reciprocal of the relative noise and so expresses the same concept as the signal to noise ratio.<sup>14</sup>

$$\sigma = \sqrt{N}$$

Equation 1. The standard deviation of the counts per pixel in a region or image ( $\sigma$ ), equals the square root of the mean counts per pixel in a region or image ( $N$ ).

$$\text{Relative noise} = \frac{\sigma}{N} = 1/\text{SNR}$$

Equation 2. The relative noise equals the standard deviation of the counts per pixel in a region or image ( $\sigma$ ), divided by the mean counts per pixel in a region or image ( $N$ ). The relative noise also equals one divided by the signal to noise ratio.

When a large matrix is used in an image where the radiation is spread over a large area (for example the spine), there will usually be a lower number of counts per pixel, compared to an image where the radiation is arising from a small area (for example a solar projection). The image with a low number of counts per pixel will have poor spatial resolution due to noise. The effect of the noise in this image can be reduced by selecting a lower matrix, which will result in a higher number of counts per pixel, or increasing the acquisition time (not usually practical). The effect of reducing the noise by decreasing the matrix has to be balanced against the reduction of spatial resolution due to reducing the matrix.<sup>27</sup>

### *Image artefacts*

There are various artefacts arising from the gamma camera that will reduce spatial resolution, these include defects or cracks in the camera crystal, poorly balanced or non-functional photomultiplier tubes or faulty positioning circuitry.<sup>28</sup>

### *Spatial resolution in equine bone phase scintigrams*

When performing bone phase scintigrams there is a trade off between image quality and the logistics of the examination. By using long acquisition times, it is possible to acquire scintigrams that have high spatial resolution, although the spatial resolution of the collimator and the camera crystal will always be limiting factors. Long acquisition times can result in problems with motion blur from patient movement and higher radiation exposure to staff.<sup>3,11</sup> A diagnostically acceptable scintigram should provide enough information so that areas of abnormal bone metabolism can be identified and there is enough anatomical information present so that a region of the abnormal uptake can be localised in the

skeleton. Radiology is usually a much quicker, simpler, and safer method of obtaining detailed morphological information regarding the skeleton.

## **Contrast and density resolution of scintigrams**

### *Summation*

Equine bone phase scintigrams usually have poor contrast. Summation of emitted radiation from two objects in the plane of the radiation detected by the gamma camera will occur in a scintigram whether or not the objects are in contact. This is different to radiology where summation of opacities only occurs if two objects with the same opacity are in contact. Thus, there are more summation effects of superimposed skeletal structures in a scintigram, compared to a radiograph of the same area. This also means that in scintigrams the borders of superimposed skeletal structures cannot usually be separated. If there is a large difference in the RU of the two objects, it is usually possible to define the object with the higher RU.

### *Colour displays and digital filtering*

Due to the inherent poor contrast of bone scintigrams, colour displays and digital filtering are often used to increase image contrast compared to grey scale images. Colour displays use different shades of colour rather than the traditional image, which uses different shades of grey. A colour display increases the ability of the eye to detect contrast in the scintigram, although in some situations this might result in an increase in false positive diagnoses.<sup>15,25</sup>

Digital filters are mathematically based post-processing techniques that change the value of selected pixels to enhance the contrast and reduce the noise in scintigrams.<sup>25</sup> The Metz filter is one of the most commonly used digital filters in skeletal scintigraphy, and it has been shown to improve lesion detectability in equine scintigrams.<sup>29</sup>

### *Density resolution*

The contrast of the scintigram image is also determined by the density resolution, that is, the number of counts that can be stored in each pixel. Currently most scintigraphic software is 8 bit (byte), but 16 bit (word) mode is also available. An 8 bit image has  $2^8$  (256) different possible values. The human eye can only distinguish about 30 shades of grey<sup>30</sup>, thus the range of shades of grey in an 8 bit image can be beyond the range of detection of the human eye. When a colour scale is used with three colours, then each colour has  $2^8$  (256) different values; this is called 24 bit colour.<sup>15</sup> Due to the huge range of shades and colours possible from an 8 bit grey scale or 24 bit colour display it is very unlikely that increasing the density resolution will change the appearance of the scintigram image to the human eye.

### *Signal and noise*

The same principles that apply to spatial resolution apply to contrast resolution (see above).

## **The navicular bone**

The navicular bone is located on the palmar aspect of the distal interphalangeal joint. The dorsal surface is covered with a smooth layer of articular cartilage, has a central eminence flanked by concave areas and articulates with the palmar aspects of the condyles of the middle phalanx. The distal border has on its dorsal aspect a narrow facet for articulation with the distal phalanx.<sup>31</sup>

Three ligaments make up the navicular suspensory apparatus. The lateral and medial collateral sesamoidean ligaments firmly attach the proximal, lateral, and medial borders of the navicular bone to the proximal phalanx, middle phalanx and the cartilage of the distal phalanx. The distal sesamoidean impar ligament firmly attaches the distal border of the navicular bone to the flexor surface of the distal phalanx.<sup>32,33</sup> The distal sesamoidean impar ligament blends with the deep digital flexor tendon immediately proximal to their insertions.<sup>33</sup>

The palmar surface of the navicular bone is also covered with articular cartilage, and forms part of the dorsal margin of the navicular bursa. The deep digital flexor tendon passes across the palmar surface of the navicular bone palmar to the navicular bursa, and curves dorsodistally to attach to the flexor surface and semilunar crest of the distal phalanx.<sup>31-33</sup> Further anchorage of the navicular bone is provided by the deep digital flexor tendon that exerts a force in a dorsal direction on the navicular bone. This force is greatest during the propulsive phase of the stride.<sup>34</sup>

### **Navicular disease**

Navicular disease is a chronic, usually bilateral, forelimb lameness that is associated with pain arising from the navicular bone and its closely related structures.<sup>35</sup> It is estimated that navicular disease is responsible for one-third of all chronic forelimb lameness in horses.<sup>36</sup> The pathogenesis of navicular disease is incompletely understood, although there are two major theories. The theories are; it is a vascular problem, and/or it has a biomechanical origin.<sup>37</sup> The main diagnostic methods currently used for navicular disease are; clinical examination findings, local analgesic techniques, radiology, scintigraphy and magnetic resonance imaging.<sup>35</sup>

### **Navicular disease and scintigraphy**

Navicular disease was one of the abnormalities described in the first report on scintigraphy in horses in the late 1970s.<sup>4</sup> Since then, there have been many publications on the scintigraphic changes seen in navicular disease.<sup>1-13,20</sup> Scintigraphy is more sensitive at detecting navicular disease than radiology, but both techniques have a nearly equal specificity.<sup>5</sup> The highest sensitivity and specificity are achieved when radiographs and scintigrams are evaluated together.<sup>5</sup>

Three projections are usually taken in a routine bone phase scintigraphy examination of a front foot; a lateral projection, a dorsopalmar projection and a solar projection. The lateral and solar projections are examined when evaluating the navicular bone region. When an IRU is seen in the navicular region in one of



these projections often an IRU will be seen in the navicular region in the other projection, but this is not always the case.<sup>2,5</sup> The solar scintigram is the most sensitive projection for detecting navicular disease.<sup>1</sup>

Soft tissue phase images of the navicular region have also been investigated.<sup>2,5</sup> Lateral soft tissue phase images are considered useful in the evaluation of navicular disease<sup>5</sup>, but solar soft tissue phase images do not help in the diagnosis of navicular disease.<sup>2</sup>

### **The solar projection scintigram**

The solar projection of the front foot was first mentioned by Ueltshi in 1977.<sup>4</sup> This report described placing the front foot on the surface of the gamma camera to take an image of the solar region of the foot with the minimum attenuation of the radiation by soft tissue and minimum superimposition of surrounding skeletal structures. Since this first report, there have been numerous references made to the solar projection of the front feet.<sup>2-13,20</sup>

Various descriptions exist on how the solar projection of the front feet should be positioned in sedated standing horses. In all descriptions, the sole of the foot is placed on the face of the horizontally positioned gamma camera.<sup>2,3,8,11,21</sup> Descriptions vary from elevating the limb and placing the sole of the foot directly on the face of the gamma camera<sup>2</sup>, to positioning the horse so it stands on the face of the gamma camera<sup>3</sup>. Some publications mention that the front limb or digit should be extended when positioning the solar projection.<sup>8,21</sup> The most thorough description of the solar projection describes positioning the face up surface of the gamma camera at or just below the level of the carpus, and stretching the forefoot out cranially and placing it on the camera face.<sup>11</sup>

### **Superimposition of other body regions on the navicular region**

The superimposition of radiopharmaceutical uptake from other anatomical regions on the navicular region is a recognised problem in solar scintigrams.<sup>2,11</sup> Superimposition of the proximal interphalangeal joint on the navicular bone region resulted in a substantial number of false positive increases in radiopharmaceutical uptake in the navicular bone region.<sup>2</sup> It is recommended that the limb should be extended when taking the solar projection, to avoid summation of the RU of the metacarpophalangeal joint and the proximal interphalangeal joint.<sup>8,21</sup> The head should be held to one side when acquiring the solar projection to avoid summation of counts from this region with the foot.<sup>21</sup> It is mentioned that a lead shield may be placed over the distal part of the limb during acquisition of the solar projection to avoid summation of radiopharmaceutical uptakes (RUs) from other areas.<sup>3,8,21</sup> Performing the solar projection with the horse standing over the gamma camera is reported to cause superimposition of the pastern and fetlock over the navicular bone region.<sup>11</sup>

### **Count acquisition for the solar scintigram**

The suggested required counts for solar projection images to be diagnostically acceptable range from 15 000-25 000 counts<sup>5</sup>, 100 000 counts (matrix 128 x 128)<sup>2</sup>, 100 000-150 000 counts<sup>11</sup>, a minimum of 150 000 counts (matrix 256 x 256)<sup>8</sup>, 200

000 counts.<sup>7</sup> This is a large variation for a factor that is very important to the spatial resolution of the scintigram. Further research on this topic would be helpful.

### **Evaluation of the solar scintigram**

The criterion for subjective evaluation of the navicular region in the solar scintigram is that in normal horses the navicular region should have the same or slightly more intensity than the distal phalanx.<sup>5</sup> Thus, the navicular bone should not normally be seen as a discrete structure in a solar scintigram.<sup>21,24</sup> If there is an IRU in the navicular bone region the degree, position and whether the IRU is focal or diffuse should be described. Some authors consider a mild diffuse IRU in the navicular bone region to be a normal variation in certain breeds, but a mild focal IRU to be abnormal.<sup>38</sup> Moderate to severe IRUs in the navicular bone region indicate an abnormality.<sup>38</sup>

There have been a series of publications investigating techniques of quantitative evaluation of the navicular bone region.<sup>2,7,8,10,13</sup> The most common technique is to draw a ROI around the navicular bone region and compare this to a ROI drawn on a region of the distal phalanx<sup>2,8,10,13</sup> or a ROI drawn on a region of the middle and proximal phalanges.<sup>10</sup> Techniques are also described where a profile is placed perpendicular to the axis of the leg, including the palmar processes and the navicular regions.<sup>7,13</sup> Ratios are calculated from the ROI techniques between the navicular region and the other (reference) regions, the aim being to have a normal range of ratios and an abnormal range of ratios. The profile techniques are evaluated by examining the shape of the profile graph and the relative height of the peaks.

Studies have attempted to identify normal and abnormal ranges by evaluating solar projection scintigrams of horses not suspected to have navicular disease compared to horses that are clinically suspected to have navicular disease. Mean values of the ratios from normal and abnormal horses have been published.<sup>2,7,8</sup> These studies have compared these ratios to subjective evaluation of the scintigrams, and to other diagnostic tests for navicular disease. The confidence in the use of these ratios has varied from limited with too many false positive results region<sup>7</sup>, to fairly good<sup>8</sup>, and good.<sup>2</sup>

### **Positioning the navicular region of interest**

There have been various methods used by these studies to identify the navicular bone region. Radiographs of the foot taken with the same positioning as the solar projection have been used to position the navicular ROI.<sup>2</sup> The palmar processes in the scintigram have been used to guide the positioning of the navicular ROI.<sup>7</sup> Some studies do not describe how the ROI were positioned<sup>8,10,13</sup>, although one of these studies mentions that observations in previous clinical cases were used to select the ROIs.<sup>8</sup> Therefore, it is not possible to compare the results from the different studies and there is likely variation between the studies on the location of the navicular ROI. No published studies describe an accurate and repeatable method that can be used in multiple horses for positioning a navicular ROI in the solar projection.

If the navicular ROI is not located accurately in the area of the navicular bone in the solar scintigram, then the ratios calculated from quantitative techniques will not give a true ratio for the navicular bone. The conclusions from such quantitative measurements could be inaccurate.

## References

1. Lamb CR, O'Callaghan MW. Combined modality imaging of the equine musculoskeletal system. In: Berry CR and Daniel GB, Eds. *Handbook of Veterinary Nuclear Medicine*. North Carolina, North Carolina State University; 1996: 49-59.
2. Keegan KG, Wilson DA, Lattimer JC, Twardock AR, Ellersieck MR. Scintigraphic evaluation of <sup>99m</sup>Tc-methylene diphosphate uptake in the navicular area of horses with lameness isolated to the foot by anaesthesia of the palmar digital nerves. *AJVR* 1996;57:415-421.
3. Ross MW, Stacy VS. Nuclear Medicine. In: Ross MW, Dyson SJ, eds. *Diagnosis and Management of Lameness in the Horse*. St Louis, United States of America: Saunders; 2003:198-212.
4. Ueltschi G. Bone and joint imaging with <sup>99m</sup>Tc labelled phosphates as a new diagnostic aid in veterinary orthopaedics. *J Am Vet Radiol Soc* 1977;18:80-84.
5. Trout DR, Hornof WJ, O'Brien TR. Soft tissue- and bone-phase scintigraphy for diagnosis of navicular disease in horses. *JAVMA* 1991;1:73-77.
6. Turner TA. Differentiation of navicular region pain from other forms of palmar heel pain. *Pferdeheilkunde* 1996;12:603-606.
7. Ueltschi G. Stellenwert der Knochenszintigraphie und der Röntgenuntersuchung beim Problemerkis der Podotrochlose. *Pferdeheilkunde* 1999;15:122-128.
8. Dyson S. Subjective and quantitative scintigraphic assessment of the equine foot and its relationship with foot pain. *Equine Vet J* 2002;34:164-170.
9. Dyson S, Marks D. Foot pain and the elusive diagnosis. *Vet Clin Equine* 2003;19:531-565.
10. Schwan M, Gerlach, Jahn W, Sill V. Quantitative assessment of nuclear bone scans using the regions of interest technique as applied to the navicular bone and insertion of the deep digital flexor tendon regions of interest in the distal phalanx of the horse. In: *Proceedings of the 12th Annual Conference of the European Association of Veterinary Diagnostic Imaging*. 2005:41.
11. Steyn PF. Nuclear medicine. In: Stashak TS, ed. *Adams' Lameness in Horses*. Philadelphia, United States of America: Lippincott Williams and Wilkins; 2002:347-375.
12. Devous MD, Twardock AR. Techniques and applications of nuclear medicine in the diagnosis of equine lameness. *JAVMA* 1984;184:318-325.
13. Lauk HD, Wanschura C. Scintigraphic evaluation of the navicular bone compared to distal toe joint angulation, hoof geometry, clinical and radiographic findings of navicular disease in 105 horses. In: *Proceedings of the 5th Annual Conference of the European Association of Veterinary Diagnostic Imaging*; 1998:6.
14. Bushberg JT, Seibert JA, Leidholdt EM, Boone JM. *The Essential Physics of Medical Imaging*. Philadelphia, Lippincott Williams and Williams; 2002.
15. Hornof WJ. An introduction to computer processing of planar scintigraphic images. In: Berry CR and Daniel GB, Eds. *Handbook of Veterinary Nuclear Medicine*. North Carolina, North Carolina State University; 1996: 25-35.
16. Fuji Photo Film Co. Ltd., FCR (Fuji Computed Radiography) General Description of Image Processing. Tokyo. Fuji Photo Film Co. Ltd; 2002.
17. Elliott AT. Quality control. In: Sharp PF, Gemmell HG, Smith FW, eds. *Practical Nuclear Medicine*. Oxford, United Kingdom: IRL Press at Oxford University Press; 1989:15-27.

18. Thrall DE, Widmer WR. Radiation physics, radiation protection, and darkroom theory. In: Thrall DE ed. *Textbook of Veterinary Diagnostic Radiology*. Philadelphia, WB Saunders Company; 2002:15.
19. Krupinski EA. Softcopy interpretation. *EMedicine*. January 19, 2005. <http://www.emedicine.com/radio/topic872.htm>; pp1-9 (accessed 29-Dec-2005).
20. Chambers MD. Bone Imaging: The Diphosphonates. In: Berry CR and Daniel GB, Eds. *Handbook of Veterinary Nuclear Medicine*. North Carolina, North Carolina State University; 1996: 49-59.
21. Pilsworth RC, Dyson SJ. Practical scintigraphic examination of the horse. In: Dyson SJ, Pilsworth RC, Twardock AR, Martinelli MJ, eds. *Equine scintigraphy*. Newmarket, United Kingdom: Equine Veterinary Journal Ltd; 2003:73-75.
22. Driver AJ. Basic principles of Equine Scintigraphy. In: Dyson SJ, Pilsworth RC, Twardock AR, Martinelli MJ, eds. *Equine scintigraphy*. Newmarket, United Kingdom: Equine Veterinary Journal Ltd; 2003:17-24.
23. Kowalsky RJ. Principles of radioactive decay, radioactivity, <sup>99m</sup>Tc generator and radiopharmacy. In: Berry CR and Daniel GB, Eds. *Handbook of Veterinary Nuclear Medicine*. North Carolina, North Carolina State University; 1996: 1-17.
24. Twardock RA. Basic structure and function of the camera. In: Dyson SJ, Pilsworth RC, Twardock AR, Martinelli MJ, eds. *Equine scintigraphy*. Newmarket, United Kingdom: Equine Veterinary Journal Ltd; 2003:42.
25. Weeks J, Dyson SJ. Image acquisition, post processing, display and storage. In: Dyson SJ, Pilsworth RC, Twardock AR, Martinelli MJ, eds. *Equine scintigraphy*. Newmarket, United Kingdom: Equine Veterinary Journal Ltd; 2003:53-68.
26. Dyson SJ. Patient preparation. In: Dyson SJ, Pilsworth RC, Twardock AR, Martinelli MJ, eds. *Equine scintigraphy*. Newmarket, United Kingdom: Equine Veterinary Journal Ltd; 2003:69-71.
27. Daniel GB, Berry CR. The Gamma Camera. In: Berry CR and Daniel GB, Eds. *Handbook of Veterinary Nuclear Medicine*. North Carolina, North Carolina State University; 1996: 1-17.
28. Daniel GB, Poteet B, Kowalsky RD. Image artefacts and quality control. In: Berry CR and Daniel GB, Eds. *Handbook of Veterinary Nuclear Medicine*. North Carolina, North Carolina State University; 1996: 36-44.
29. Eksell P, Carlsson S, Lord P, Carlsten J. Effects of a digital filter on detectability of a phantom lesion in a scintigram of the equine tarsus. *Vet Radiol Ultrasound*. 2000;41:365-370.
30. Russ JC. Acquiring images. In *The Image Processing Handbook*. Boca Raton: CRC Press Inc; 1995:1-70.
31. Getty R. Sisson and Grossmans, *The Anatomy of Domestic Animals*. Philadelphia. W.B. Saunders Company. 1975.
32. Kainer RA. Functional Anatomy of Equine Locomotor Organs. In: Stashak TS, ed. *Adams' Lameness in Horses*. Philadelphia, United States of America: Lippincott Williams and Wilkins; 2002:1-72.
33. Bowker R. Functional anatomy of the palmar aspect of the foot. In: Ross MW, Dyson SJ, eds. *Diagnosis and Management of Lameness in the Horse*. St Louis, United States of America: Saunders; 2003:282-286.
34. Dyson SJ. Primary lesions of the deep digital flexor tendon within the hoof capsule. In: Ross MW, Dyson SJ, eds. *Diagnosis and Management of Lameness in the Horse*. St Louis, United States of America: Saunders; 2003: 305-309.
35. Dyson SJ. Navicular disease and other soft tissue causes of palmar foot pain. In: Ross MW, Dyson SJ, eds. *Diagnosis and Management of Lameness in the Horse*. St Louis, United States of America: Saunders; 2003:286-299.
36. Colles CM. Navicular disease and its treatment. *In Practice*. 1982;4:29-35.
37. Leach DH. Treatment and pathogenesis of navicular disease ('syndrome') in horses. *Equine Vet J* 1993;25:477-481.
38. Dyson SJ. The Sports Horse. In: Dyson SJ, Pilsworth RC, Twardock AR, Martinelli MJ, eds. *Equine scintigraphy*. Newmarket, United Kingdom: Equine Veterinary Journal Ltd; 2003:191-224.

# **THE RADIOGRAPHIC LOCATION OF THE EQUINE NAVICULAR BONE IN THE FRONT LEGS, THE EFFECT OF LEG POSITIONING, AND A METHOD TO POSITION A NAVICULAR BONE REGION OF INTEREST IN A SOLAR SCINTIGRAM**

**Charles J. Ley, Per Eksell**

The anatomical location of the navicular bone and the amount of superimposition of the region of the proximal interphalangeal joint (PIPJ) on the navicular bone has not been clearly established in solar projection scintigrams. Using radiographs of the front legs of horses, this study investigated movement of the navicular bone relative to the distal phalanx with changes in pastern angle, navicular bone position relative to landmarks on the distal phalanx, and superimposition of the PIPJ on the navicular bone. Leg positioning did not change the position of the navicular bone relative to the distal phalanx in a dorsal to palmar plane. Little variation existed between individuals in: the ratio of the distance from the dorsodistal margin of the distal phalanx to the dorsal margin of the navicular bone (P3-Navicular) compared to the dorsopalmar length of the navicular bone (Navicular length), the ratio between the maximum lateral width of the distal phalanx (P3 width) and P3-Navicular, and the ratio between P3 width and the maximum lateral width of the navicular bone (Navicular width). In contrast, large variation existed in the ratio of the distance from the palmar aspect of the palmar processes to the palmar aspect of the navicular bone (Navicular-PP), compared to Navicular length. Positioning the pastern in maximum flexion resulted in the least overlap of the proximal interphalangeal joint and navicular regions. This information was applied to a solar projection scintigram to locate a navicular bone region of interest. It is recommended that the phalanges are flexed and the sole is placed flat on a raised horizontal gamma camera when the solar projection is acquired.

## **Introduction**

The solar projection is the most sensitive scintigraphic projection for detecting abnormalities in the navicular bone<sup>1</sup>. The solar projection of the front feet is positioned by moving the gamma camera so the receiving surface (face) is approximately horizontal and placing the foot onto the face of the gamma camera. It is recommended that the limb should be stretched out cranially to avoid superimposition of the fetlock and pastern<sup>2,3</sup>. Considerable variations exist in the gamma camera gantries and the rooms where scintigraphy is performed at equine scintigraphy clinics<sup>4,5</sup>. This has resulted in many different methods of positioning the solar projection, varying from the horses standing bearing full weight on the face of the gamma camera<sup>4</sup>, to methods where the leg is pulled forward and placed on the face of a raised gamma camera<sup>2</sup>.

Abnormalities of the navicular bone are common causes of foot pain in horses. When available, skeletal scintigraphy is a common diagnostic technique for localising skeletal causes of lameness in the equine distal limb when clinical

examination, radiology, or ultrasound examinations are unable to provide a diagnosis. Reports on scintigraphic examination of the equine foot describe abnormal radiopharmaceutical uptake (RU) patterns in the navicular bone and attempt to relate these patterns to specific diseases and syndromes<sup>1,6-12</sup>, however, there are no studies that confirm the location of the navicular bone in the solar projection image. A technique is described where radiographs were taken with the foot positioned identically as that for obtaining corresponding scintigraphic images, and templates are made from these radiographs, which are then superimposed on the scintigrams to identify the navicular region<sup>1</sup>. This technique has the disadvantages that a radiograph needs to be taken of each foot that is examined, and unless radiographs are taken during the positioning of the foot for the scintigram, there will likely be some variation in the foot positioning for the radiographs.

If the exact position of anatomical structures in the scintigraphy images is unknown, there is a risk that regions of abnormal RU pattern can be interpreted as arising from one anatomical structure, when they have actually arisen from another. The need for such anatomical localisation in scintigrams is demonstrated by a recent study<sup>14</sup> concerning the sacroiliac joint region.

Bone phase scintigrams provide detailed skeletal functional information but poor anatomical detail. Prominent anatomical landmarks in the scintigram that have a characteristic shape or RU can be used to estimate the position of smaller and poorly defined anatomical structures. Unless there is a marked increase in radiopharmaceutical uptake (IRU) in the navicular bone, the margins of the navicular bone often cannot be clearly defined in the solar projection scintigram. The palmar processes of the distal phalanx can be used to estimate the location of the navicular bone both when examining the image subjectively and when drawing ROIs for objective measurements<sup>9</sup>. The relation between the positions of the palmar processes of the distal phalanx and the navicular bone in the solar projection and whether the positions of these structures are consistent between horses have not been thoroughly investigated. Other anatomical structures such as the solar margin of the distal phalanx could also be used to help localise the position of the navicular bone, but no mention is made in the literature of how or if such structures are used.

Studies that have investigated techniques of quantitative scintigraphic assessment of the equine foot using regions of interest (ROIs) do not describe a specific method for determining the location of the navicular bone ROI<sup>9,10,12</sup>. For these quantitative techniques of measurement to be correct, the location of the navicular bone ROI must be accurate.

The effect on the position of the navicular bone by the angle of the pastern to the gamma camera in the solar projection has not been investigated. It is not known whether different techniques of performing the solar projection result in different positions of the navicular bone relative to the distal phalanx.

Superimposition of adjacent skeletal structures results in summation of the radioactivity and thus an apparent IRU. It is desirable to avoid superimposition in skeletal scintigrams since this may result in an incorrect diagnosis of a bone lesion. The proximal interphalangeal joint (PIPJ) is able to move dorsal and palmar in an axial plane relative to the navicular bone, thus the degree of superimposition of the PIPJ region and navicular bone region will change

depending on the degree of flexion or extension of the joints of the distal limb. Superimposition of RUs arising from the PIPJ on the navicular bone is reported as a reason for false positive diagnosis of IRUs in the navicular bone region in the solar projection scintigram<sup>1</sup>. Superimposition of the PIPJ and metacarpophalangeal joint regions on the navicular bone region is described as occurring when the solar projection is taken with the horse standing on the gamma camera<sup>2</sup>.

To accurately identify the position of the navicular bone this study required an imaging technique with good skeletal resolution, thus radiographs were used. Since the solar projection scintigram is based on gamma radiation that is orientated perpendicular to the weight-bearing surface of the hoof, it is possible to extrapolate position measurements done at 90° to the weight-bearing surface of the hoof in lateral to medial (LM) radiographic projections to these scintigrams. A proximal to distal (PrDi) radiograph of the foot should result in an image that is the radiographic equivalent to a solar projection. To investigate the effect of change in angles of the pastern on the superimposition of navicular bone and the PIPJ regions, radiographs of anatomical specimens were used. To study the relative position of the distal phalanx to the navicular bone radiographs from both anatomical specimens, and from a retrospective study of radiographs of the distal front limbs of cases from the Division of Diagnostic Imaging\* clinic files were used. The information obtained from the radiographs was then used to position a navicular bone ROI in a solar projection scintigram.

The hypotheses were that due to the firm ligamentous attachments of the navicular bone and the position of the surrounding anatomical structures, there would be minimal movement of the navicular bone relative to the distal phalanx. This limited movement would allow landmarks on the distal phalanx to be used as a guide for identifying the position of the navicular bone. It was suspected that the angle of the pastern would influence the amount of superimposition of the PIPJ region on the navicular region, and that maximum flexion of the pastern would minimise, and maximum extension of the pastern would maximise this superimposition.

The objectives of this study were to find a method to position a navicular bone region of interest in solar projection images, and to investigate the degree of superimposition of the proximal interphalangeal joint region on the navicular bone region.

## **Materials and Methods**

### *Radiographic equipment*

Radiographs were taken with an x-ray tube<sup>†</sup> mounted on an overhead gantry, using a 150 kV, 3-phase generator<sup>‡</sup>, recorded on digital image plates<sup>§</sup>, processed with a computed radiography system<sup>||</sup> and viewed on a dedicated workstation with a picture archiving communication system (PACS)<sup>¶</sup>. The exposure values were 55 kVp and 100 mAs for all lateral projections and 102 kVp and 32 mAs for all proximal to distal projections. The film focal distance was 125 cm. The measurements of angles and distances were made with the tools available in the PACS<sup>¶</sup>.

### *Anatomical specimens*

Thirteen front limbs disarticulated at the carpometacarpal joints and two front limbs disarticulated at the metacarpophalangeal joints were obtained from euthanased horses. No information was available regarding the age, breed, or previous use of the horses, but in all legs, the physes of the phalanges were closed. The specimens were frozen within 24 hours of euthanasia of the horses and completely thawed before taking the radiographs.

### *Radiographs of clinical cases (live horses)*

LM radiographs of the distal front limbs of live horses that had been taken at the Division of Diagnostic Imaging clinic\* between February 2005 and October 2005 were measured. The horses were positioned with the foot on a 10cm high wooden block and the x-ray cassette was positioned as close to the medial margin of the hoof as possible. The x-ray beam was horizontal, and the x-ray cassette parallel with the leg. There was a variation in how much weight the horses were bearing when the radiograph was taken, some were fully weight bearing others had minimal weight on the foot. Any cases that had a diagnosis of laminitis, abnormal foot conformation or displaced fractures were excluded. Radiographs from horses where the proximal physis of the middle phalanx was not closed were excluded. No oblique projections were included. Twenty-seven distal front limb radiographs from clinical cases were identified that fitted the inclusion criteria. These radiographs were from 22 live horses. Seventeen horses had one front foot radiographed, five horses had both front feet radiographed. The breeds of horse included; Warmblood (10), Thoroughbred (3), Quarter horse (2), Standardbred (1), Coldblood Trotter (1), Lusitano (1), Andalusier (1), Haflinger (1), North Swedish Farm horse (1) and a crossbred (1). The age of the horses ranged from 18 months to 17 years, the mean age was 8.1 years.

### *Preparation of anatomical specimens*

In the thirteen legs disarticulated at the carpometacarpal joint, holes were drilled in the dorsal aspect of the third metacarpal bone approximately 5cm proximal to the metacarpophalangeal joint and in the palmar aspect of the third metacarpal bone approximately 3cm distal of the proximal articular surface of the third metacarpal bone. Wood screws (4.5mm x 50mm) were screwed into the drilled holes to act as attachment points for ropes used to position the legs (Figure 1). In the two legs disarticulated at the metacarpophalangeal joint, no screws were fixed to the skeleton.



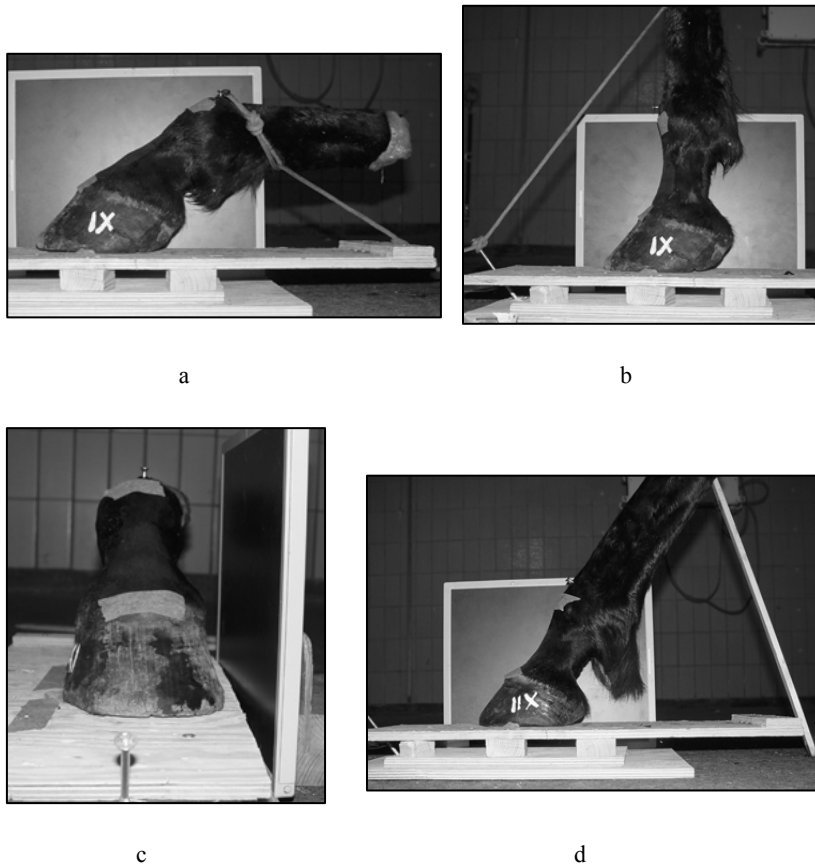


Figure 1. The positioning of the specimen legs for LM radiographs. The hooves are attached to a wooden board with screws and held in maximum flexion (a) and maximum extension (b) with a rope. (c) A specimen leg positioned for a LM radiograph seen from the dorsal aspect. (d) A specimen leg in the 50° position, the leg is held in position by a piece of wood supporting the palmar aspect of the proximal metacarpus.

The hooves were cleaned and firmly attached to a 25x22cm rectangular piece of 12mm thick plywood with four wood screws (4.0x35mm), which were placed in the medial, lateral, dorsomedial and dorsolateral hoof walls. The hooves were positioned so that either the lateral or the medial margin of the hoof was close to the edge of the plywood (thus the x-ray cassette could be placed as close as possible to the foot). The long axis of the legs was approximately parallel to the long axis of the plywood. This rectangular piece of plywood was then attached to a 25x55cm piece of plywood using wood screws, and with 2cm thick wood blocks between the two pieces of plywood, which acted as spacers so that an x-ray cassette could be easily placed under the hoof. Screws were attached in the middle of the short ends of the plywood and these acted as attachment points for ropes used to position the legs in flexion and extension. Tape<sup>#</sup> was used to position the two legs that were disarticulated at the metacarpophalangeal joint in flexion and extension, thus no screws were used as anchor points.

### *Positioning of the radiographs of the specimens*

LM radiographs of the each distal limb were taken in three different positions; maximum flexion, maximum extension, with the dorsal aspect of the middle phalanx at  $50^\circ \pm 1^\circ$  to the weight bearing surface of the hoof (Figure 1 and 2). The x-ray cassette was held in a constant position beside the foot by placing it between the foot and a wood block. Projections were centred on the coronary band on the lateral aspect of the foot and collimated so that the entire hoof and proximal phalanx were included. The x-ray camera was positioned so the x-ray beam was

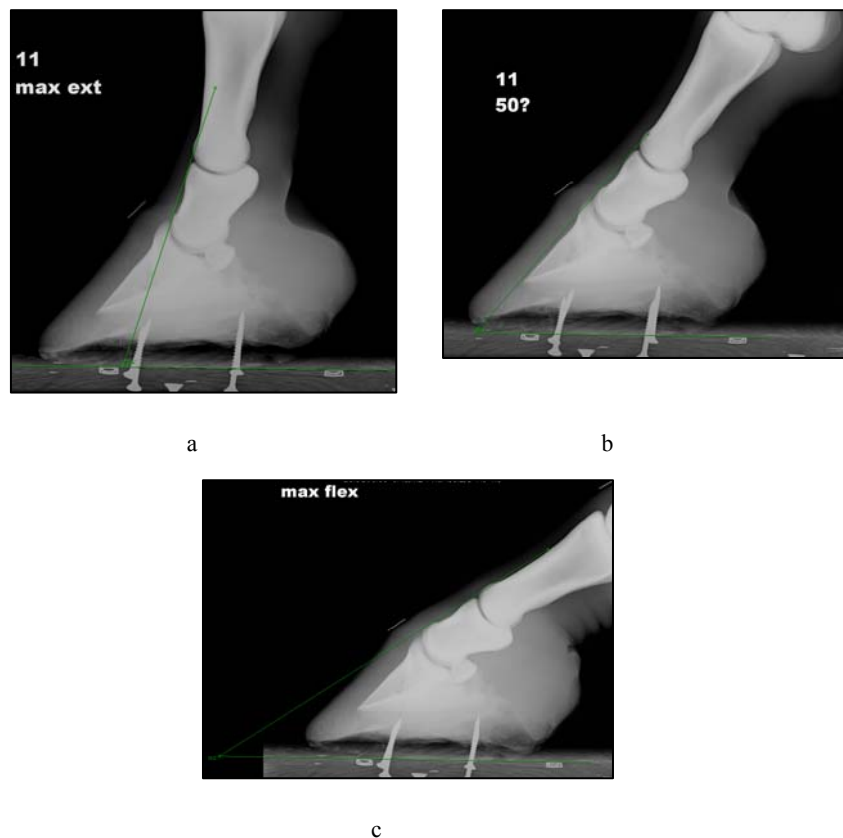


Figure 2. LM radiographs of the specimen legs in (a) maximum extension, (b) in the  $50^\circ$  position and (c) maximum flexion. The angles of the legs were measured from a line drawn between the two metal markers attached to the wooden board.

horizontal. The legs were positioned so the condyles of the middle phalanx were superimposed in the radiograph. The  $50^\circ$  LM radiographs were done by estimating the correct position of the leg, taking the radiograph, and measuring the angle between the weight bearing surface of the hoof and the dorsal aspect of the middle phalanx on the radiographs. If the angle was not  $50^\circ$  the position of the leg was

then changed according to the angle measured and the radiograph repeated until an angle of  $50^{\circ} \pm 1^{\circ}$  was achieved.

PrDi radiographs of the distal limb were centred on the dorsal aspect of the coronary band and taken at maximum flexion immediately after the LM radiograph had been taken in this position (Figure 3). The leg remained in exactly the same position in these two projections. The camera was positioned so the x-ray beam was vertical and the x-ray cassette was positioned under the foot between the two pieces of plywood.

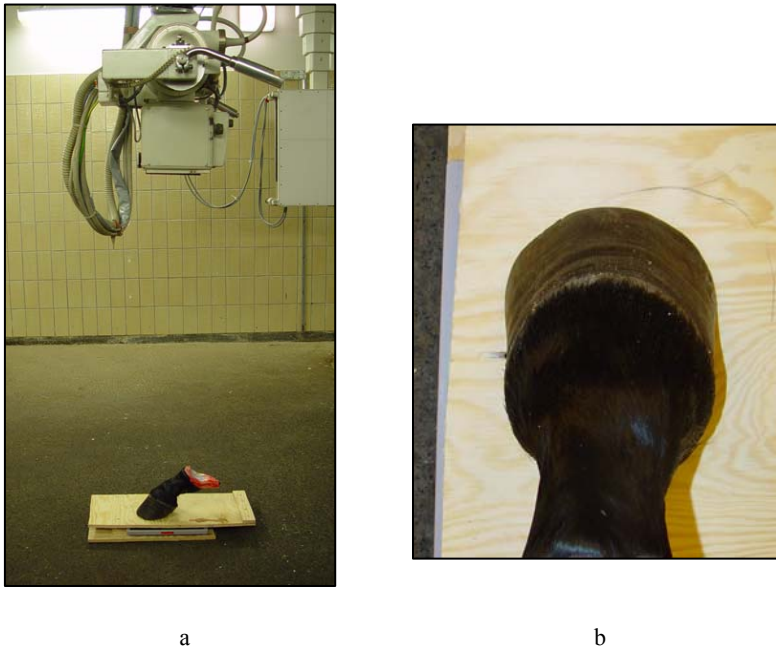


Figure 3. The positioning of the specimen legs for PrDi radiographs. (a) The x-ray tube is positioned directly above the leg, with the cassette under the foot between the two pieces of wood. (b) The hoof seen at the same angle of projections as it is in the PrDi radiograph.

The legs disarticulated at the carpometacarpal joint were held in maximum extension by placing a rope tightly around the metacarpus directly proximal to the screw in the palmar surface of the third metacarpal bone. This rope was tied to the screw that was in the short end of the plywood on the dorsal side of the leg. The legs were held in maximum flexion by placing a rope tightly around the metacarpus directly distal to the screw in the dorsal surface of the third metacarpal bone. This rope was tied to the screw that was in the short end of the plywood on the palmar side of the leg. The tension on the rope holding the legs in position was done by hand and was so that the rope was taut and firm. The legs disarticulated at the metacarpophalangeal joint were held in flexion and extension by using tape<sup>#</sup>, which was wrapped around the proximal part of the proximal phalanges and firmly attached to the appropriate short end of the plywood. Once again, the tension on the tape was made manually so that the tape was taut and firm.

### *Reference line*

Measurements were made on the LM radiographs to establish a reference line fixed to the location of the distal phalanx. The use of this reference line for measurements ensured that any bending of the plywood or movement of the fixation of the hoof to the plywood would not effect the measurements. The reference line was used to measure changes in the positions of the middle phalanx, the navicular bone, and the PIPJ relative to the distal phalanx in the flexed and extended positions (Figure 4).

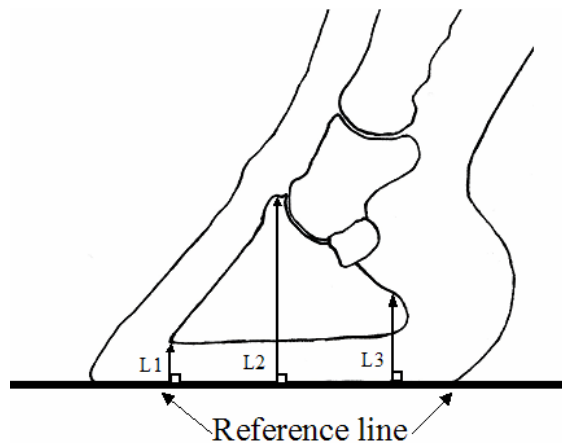


Figure 4. Measurement points were used to create the reference line for each foot. The aim of this line was that it should be in exactly the same position, relative to the distal phalanx (rather than the hoof wall), when each foot was in maximum flexion and maximum extension. Measurements were made in the maximum extension radiograph from a line drawn between the metal markers taped to the surface of the wooden board to; the distal tip of the distal phalanx (L1), the proximal margin of the extensor process of the distal phalanx (L2) and a clearly identifiable anatomical structure on the proximal margin of the palmar processes(L3). When these measurements were different between the maximum flexion and maximum extension images the line between the metal markers was moved in the maximum flexion radiograph until L1, L2 and L3 had exactly the same value as they had in the maximum extension radiograph for that foot. The adjusted line was called the reference line and this line was used for all distance measurements when investigating movement of the navicular bone, angle measurements of flexion and extension, and change in position of the navicular bone and PIPJ regions.

### *Measurements of the angles of flexed and extended lateral radiographs*

A line that joined the dorsodistal and dorsoproximal convex surfaces of the middle phalanx was drawn along the dorsal aspect of the middle phalanx. The angle between the dorsal aspect of the middle phalanx and the reference line was calculated for each maximum flexed and extended radiograph.

### *Measurements of the change in position of the navicular bone*

The LM radiographs were measured in maximum flexion and extension to investigate if there was a change in position of the navicular bone relative to the distal phalanx in a dorsal to palmar (horizontal) or proximal to distal (vertical) directions (Figure 5).

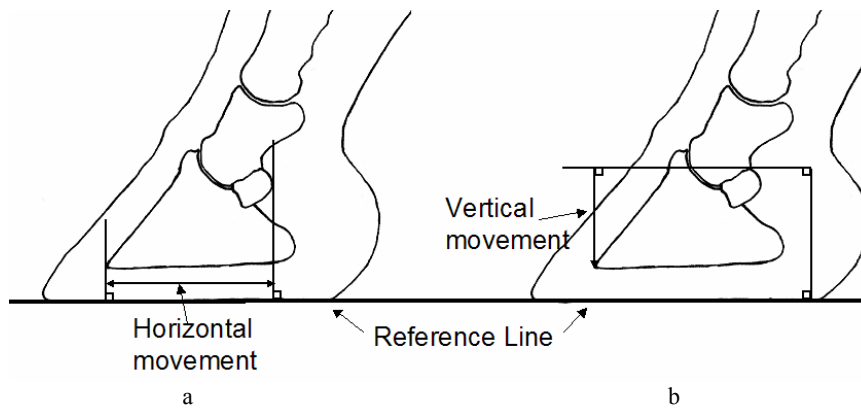


Figure 5. (a) The measurement of the dorsal to palmar distance between the dorsodistal margin of the distal phalanx to the palmar margin of the navicular bone. This measurement was done parallel to reference line and was used to measure the dorsal to palmar (horizontal) movement of the navicular bone relative to the distal phalanx. (b) The measurement of the proximal to distal distance between the dorsodistal margin of the distal phalanx to the proximal margin of the navicular bone. This measurement was done perpendicular to the reference line and was used to measure the proximal to distal (vertical) movement of the navicular bone relative to the distal phalanx.

### *Measurements of the location of the navicular bone relative to the distal phalanx in specimens and live horses in the LM radiographs*

LM radiographs were taken of specimens when the leg was in a neutral position ( $50^\circ \pm 1^\circ$ ) and of clinical cases when the horse was weight bearing. The dorsal to palmar distance from the dorsodistal margin of the distal phalanx to the dorsal margin of the navicular bone (P3-Navicular), the dorsal to palmar length of the navicular bone (Navicular length) and the dorsal to palmar distance from the palmar margin of the navicular bone to the palmar margin of the palmar processes of the distal phalanx (Navicular-PP) were measured (Figure 6a). The length P3-Navicular was calculated as a ratio in percentage of P3-Navicular plus the Navicular length. The length Navicular-PP was calculated as a ratio in percentage of Navicular-PP plus the Navicular length. When the palmar margin of the navicular bone was located palmar of the level of the palmar processes of the distal phalanx, the Navicular-PP ratio was given a negative value. The mean values of these ratios were calculated.

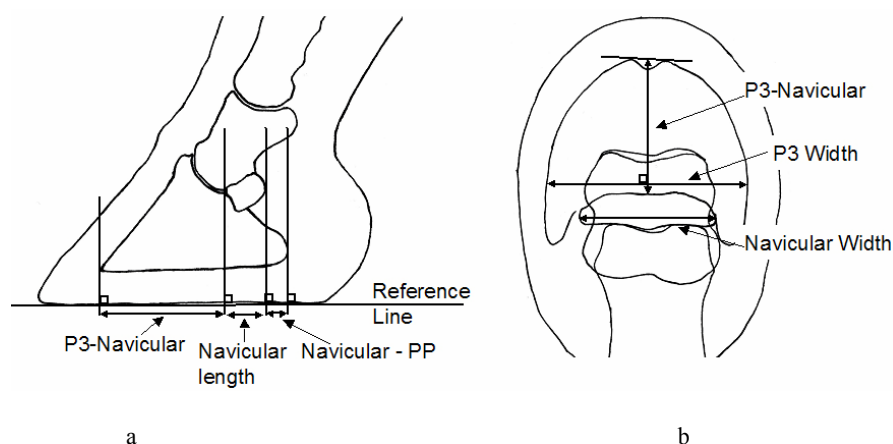


Figure 6. (a) Measurement points on the LM radiographs. P3-Navicular is the distance from the dorsodistal margin of the distal phalanx to the dorsal margin of the navicular bone. Navicular length is the distance from the dorsal to the palmar margins of the navicular bone. Navicular-PP is the distance from the palmar margin of the navicular bone to the palmar margin of the palmar processes. (b) Measurement points on the PrDi radiographs. P3-Navicular is the distance from the distal tip of the distal phalanx to the dorsal margin of the navicular bone in the axial plane. When a crena was present, a line was drawn between the dorsodistolateral and dorsodistomedial margins of the crena and the measurements taken from this line. P3 width is the maximum width of the distal phalanx taken perpendicular to the P3-Navicular line. Navicular width is the maximum width of the navicular bone taken perpendicular to the P3-Navicular line.

In each radiograph, it was noted if the palmar margin of the navicular bone was dorsal or palmar to the palmar margin of the palmar processes of the distal phalanx. If palmar margin of the navicular bone was dorsal to palmar margin of the palmar processes, the navicular bone was considered within the palmar processes.

*Measurements of the axial length of the distal phalanx dorsal to the navicular bone relative to the lateral width of the distal phalanx and the navicular bone in PrDi radiographs in specimens*

The distance from the dorsodistal margin of the distal phalanx to the dorsal margin of the navicular bone (P3-Navicular), the lateral to medial width of the distal phalanx (P3 width), and the lateral to medial width of the navicular bone (Navicular width) were measured in the PrDi projections (Figure 6b). When a crena was present, a line was drawn between the dorsodistolateral and dorsodistomedial margins of the crena, and measurements for the dorsodistal margin of the distal phalanx were made from this line (Figure 6b). The measurements of P3-Navicular and Navicular width were calculated as ratios in percentage of P3 width. The mean values of these ratios were calculated.

*Measurements of the overlap of the navicular bone and the proximal interphalangeal joint*

The dorsal to palmar lengths of the navicular bone and the PIPJ regions were measured in the maximum flexed, maximum extended and 50° LM radiographs. The amount of overlap between the navicular bone and PIPJ regions in a dorsal to palmar plane was calculated as a percentage of the length of the navicular bone (Figure 7). For the purposes of the measurements, the PIPJ region was defined as the proximal articular surface of the middle phalanx. The mean values of these percentages were calculated.

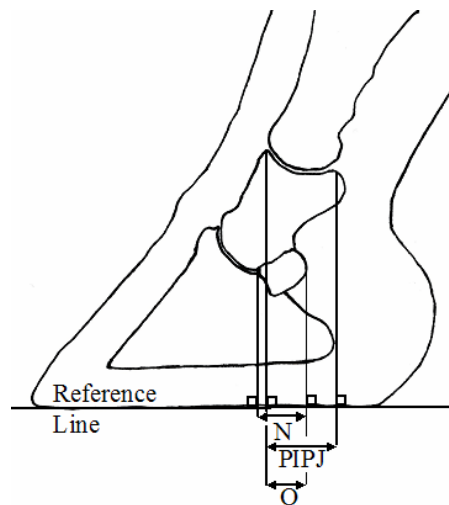


Figure 7. The measurement of the dorsal to palmar length of the navicular bone (N) and the proximal articular surface of the middle phalanx (PIPJ) and the length of overlap (O) of these two regions.

*Placement of a navicular bone region of interest on a solar scintigram using the ratios obtained from measuring the radiographs.*

The threshold setting on a solar scintigram from a routine clinical case was lowered so the solar margin of the distal phalanx could be clearly defined. The maximum lateral to medial width of the distal phalanx was measured. This value was multiplied by the P3 width/P3-Navicular ratio and this result was used to estimate the P3-Navicular value in the scintigram. Thus, the position of the dorsal margin of the navicular bone could be estimated. The estimated P3-Navicular was used to estimate the location of the palmar margin of the navicular bone using the ratio obtained in the results of the P3-Navicular and the Navicular length. The width of the navicular bone was estimated by multiplying the P3 width by the P3/navicular width ratio. Thus, the positions of the lateral and medial margins of the navicular bone were estimated (Figure 8).

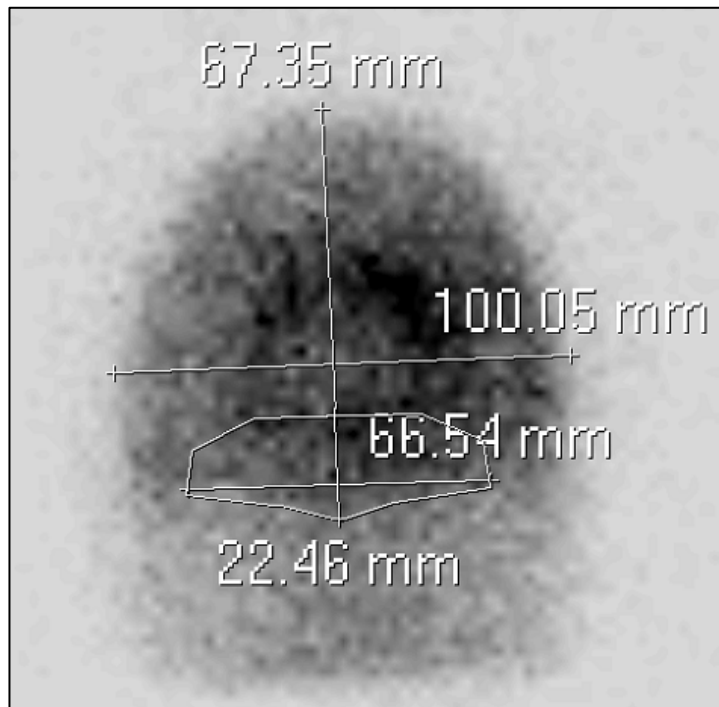


Figure 8. Example of measurements of a solar projection scintigram used to locate a navicular bone shaped ROI. The measurement of the width of the distal phalanx (100.05mm) is the basis of the calculations for the other values.

A navicular bone shaped ROI was made by tracing around the navicular bone in a PrDi radiograph. The accuracy of the shape of the ROI was confirmed by comparing the shape of the navicular ROI to the navicular bone in multiple PrDi radiographs. The estimated positions of the dorsal, palmar, lateral, and medial margins of the navicular bone were used to position a navicular bone ROI in a solar scintigram.

#### *Data analysis*

Statistical analyses were performed with a statistical software package \*\*, and statistical significance was set at  $p < 0.05$ . Normal distribution of the data was confirmed with Kolmogorov-Smirnov analysis. Paired t-tests were performed on the horizontal and vertical measurements to investigate if there was a significant difference in the position of the navicular bone relative to the distal phalanx in maximum flexion compared to maximum extension. Paired t-tests were performed on the change in amount of overlap of the navicular bone and PIPJ regions in maximum flexion, maximum extension and with a middle phalanx angle of 50°.



## Results

### *Angles of extension and flexion*

The mean angle of maximum extension was 67.9° and the standard deviation was 4.7°. The mean angle of maximum flexion was 36.4° and the standard deviation was 3.7°. The mean difference in angle of the middle phalanx to the reference line between the radiograph taken at maximum extension and the radiograph taken at maximum flexion was 31.5° and the standard deviation was 6.6°. The maximum value for the differences in angle between the radiograph taken at maximum extension and the radiograph taken at maximum flexion was 38.9° and the minimum difference was 18.7°.

### *Change in position of the navicular bone between maximum flexion and extension*

There was no significant difference between the position of the navicular bone relative to the distal phalanx in maximum extension compared to maximum flexion in a dorsal to palmar plane (horizontal movement measurement) using a paired t-test ( $p = 0.659$ ).

A significant difference ( $p < 0.001$ ) was detected between the position of the navicular bone relative to the distal phalanx in maximum extension compared to maximum flexion in a proximal to distal plane (vertical movement measurement). The mean of the difference between vertical movement in flexion and vertical movement in extension was 1.2mm with a maximum value of 3.3mm and a minimum value of -0.3mm. This indicated that navicular bone tended to move proximally relative to the distal phalanx with extension of the phalangeal joints.

### *Location of the navicular bone relative to the distal phalanx*

LM radiographs of 42 feet (15 specimens and 27 clinical cases) and PrDi radiographs of 15 feet (all specimens) were examined. The results of the measurements made on the lateral radiographs were analysed on all feet and using only the radiographs of the clinical cases (live horses). This was done since there was no information available on the age or breed of the specimens but this information was available for the live horses.

The navicular bone was within the palmar processes of the distal phalanx in 88.1% of all the legs. In the specimen radiographs, the navicular bone was within the palmar processes in 73.3% of the legs. In the live horse radiographs, the navicular bone was within the palmar processes in 96.3%, or 26 of 27 legs. The horse whose navicular bone was not completely within the palmar processes was the youngest individual in the live horse group, being approximately 18 months old. The next youngest horse in this group was three years old.

The mean value of the ratios between P3-Navicular and P3-Navicular plus Navicular length was 75% in all (specimens and live horses) legs and 74.8% in the live horses. The standard deviation was 1.5% in all legs and 1.2% in the live horses. The coefficient of variation was 2% in all legs and 1.6% in the live horses.

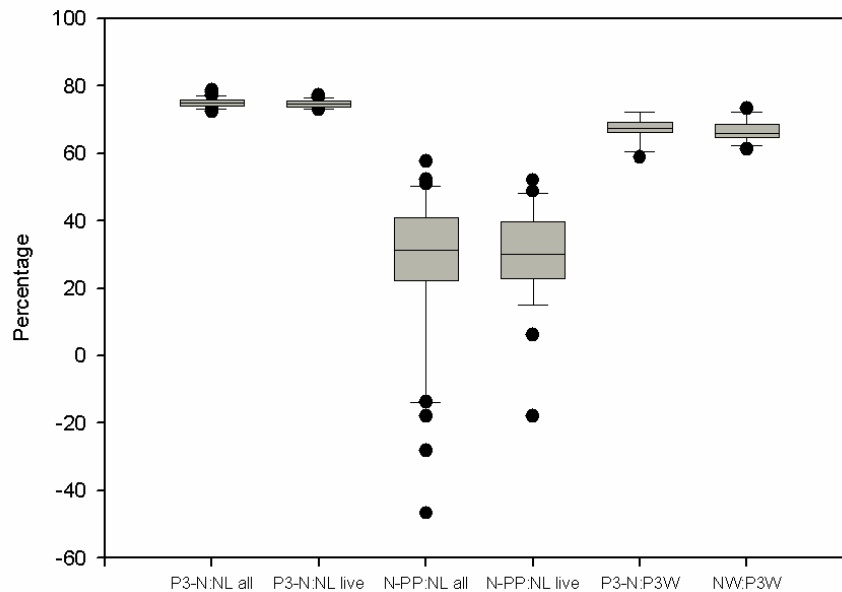


Figure 9. A box plot showing the variation of the ratios of navicular bone and distal phalanx measurements in percentage. P3-N:NL is the length of the distal phalanx dorsal of the navicular bone, compared to the dorsal to palmar length of the navicular bone. N-PP:NL is the palmar margin of the navicular bone to the palmar margin of the palmar processes of the distal phalanx, compared to the dorsal to palmar length of the navicular bone. P3-N:P3W is the length of the distal phalanx dorsal of the navicular bone, compared to the width of the distal phalanx. NW:P3W is the width of the navicular bone, compared to the width of the distal phalanx.

The ratios for P3-N:NL and N-PP:NL are shown for all legs (n=42) and for live horse radiographs only (n=27). The ratios for P3-N:NL and NW:P3W are from specimens only (n=15).

The mean value of the ratios between Navicular length plus Navicular-PP and Navicular-PP was 26.9% in all legs and 29.9% in the live horses. The standard deviation was 22.6% in all legs and 14.2% in the live horses. The coefficient of variation was 84% in all legs and 47.5% in the live horses.

The mean value of the ratios between P3-Navicular and P3 width in the PrDi radiographs of the specimens was 67.3%. The standard deviation was 3.6%. The coefficient of variation was 5.3%.

The mean value of the ratios between Navicular width and P3 width in the PrDi radiographs of the specimens was 66.6%. The standard deviation was 3.2%. The coefficient of variation was 4.8%.

A comparison of the spread of the measurements within each group using a box plot is given in figure 9.

### *Superimposition of the navicular and proximal interphalangeal joint regions*

A significant difference ( $p < 0,001$ ) was detected between the overlap of the navicular and proximal interphalangeal joint regions between all three sets of radiographs. The mean value for the percentage of the navicular region overlapped by the proximal interphalangeal joint region at maximum extension was 95.3%, at a middle phalanx angle of 50° was 48%, and at maximum flexion was 14.5%. The standard deviation of the maximum extension radiographs was 7.6%, for the 50° radiographs it was 9.1%, and for the maximum flexion radiographs it was 12.9%. In the maximum extension radiographs, 10 out of 15 legs had 100% overlap of the proximal interphalangeal joint regions and the navicular bone regions. In the maximum flexion radiographs, 5 out of 15 legs had 0% overlap of the proximal interphalangeal joint and navicular bone regions. No legs in the 50° radiographs had 100% or 0% overlap of the proximal interphalangeal joint and navicular bone regions.

### **Discussion**

The position of the navicular bone did not change in position relative to the distal phalanx in a dorsal to palmar direction when the maximum flexion and extension positions are compared. This means in the solar projection scintigram, as long as the sole of the foot is placed flat on the face of the gamma camera, the angle of the pastern will not change the position of the navicular bone relative to distal phalanx.

The position of the navicular bone relative to the distal phalanx did change in a proximal to distal direction when the angle of the pastern was changed, but this movement will not effect the relative position of the navicular bone in the solar projection scintigram. The only possible affect that this movement could have on the navicular RU is to change the shape or intensity of the RU. The amount of RU detected from a structure should not change with small changes in the source to gamma camera distance. When a source is moved away from the gamma camera the gamma rays become more parallel and the increase in the number of photons that pass through the collimator of the gamma camera is almost the same as the decrease in the photons that reach the gamma camera due to the increased distance (inverse square law).<sup>15</sup> Source object distance does affect the resolution of the scintigram but the amount of change in proximal to distal position of the navicular bone detected was much less than was required to cause a detectable difference in the image. For these reasons, the degree of movement of the navicular bone between the flexed and extended positions of the phalanges was so small that it will not cause any detectable change in the appearance of the navicular bone in solar projections.

There was a difference between the specimen group and the live horse group in the incidence of the navicular bone being within the palmar processes. In the live horse group the individual with the navicular bone that was not completely within the palmar processes was young compared to the other horses in this group. In each of the feet where the navicular bone was not within the palmar processes, the palmar processes appeared short. These findings could be due to incomplete

mineralization of the palmar processes. Thus, it is suspected that age affects the degree of overlap of the palmar processes on the navicular region in horses older than 1 year. Unfortunately, no information was available on the ages of the horses in the specimen group where four feet had this appearance. According to published ossification times of the equine skeleton the palmar processes model over 12 months<sup>16</sup>. Radiographs of the distal phalanx of horses 12 to 24 months of age could be used to investigate whether there is a regular pattern of mineralization of the palmar processes during this period.

The measurements of the ratio of the dorsal to palmar length of the palmar processes of the distal phalanx compared to the dorsal to palmar length of the navicular bone had a high coefficient of variation (84%). This showed that the palmar margin of the palmar processes of the distal phalanx were unreliable landmarks for identifying the position of the navicular bone in the solar projection. To ensure the high variation in this ratio was not a result of the high incidence of apparently short palmar processes in the specimen group, the statistics were repeated on the live horse group only and the coefficient of variation remained high (47.5%).

The ratio of the dorsal to palmar length of the distal phalanx dorsal of the navicular bone compared the dorsal to palmar length of the navicular bone showed a very low coefficient of variation (2%). This suggests that this ratio will be very useful for determining the dorsal to palmar length of the navicular bone in the solar projection. To use this ratio a method was required to estimate the distance from the dorsodistal margin of the distal phalanx to the dorsal aspect of the navicular bone. This method had to be applicable to the anatomical structures that could be clearly identified in the solar projection scintigram. The lateral margins of the distal phalanx are usually well defined in solar projections scintigrams. Measurements of the maximum lateral width of the distal phalanx were compared to the length of the distal phalanx and these measurements were found to have a low coefficient of variation (5.3%).

For construction of a navicular bone ROI, an estimate of the lateral width of the navicular bone was also required. The ratio of the lateral width of the navicular was compared to the lateral width of the distal phalanx and these measurements were found to have a low coefficient of variation (4.8%).

These ratios allow predictions of the position of the navicular bone in the solar projection. By measuring the lateral width of the distal phalanx in the solar projection, it will be possible to estimate the position of the dorsal margin of the navicular bone, and the lateral width of the navicular bone. The dorsal to palmar width of the navicular bone can then be estimated from the dorsal to palmar length of the distal phalanx dorsal to the navicular bone. It should then be possible to use the estimated dorsal, palmar, lateral and medial margins of the navicular bone to overlay a navicular bone shaped ROI using a semi-automated method and estimate the RU of this region (Figure 8).

A significant difference was present in the proportion of the navicular bone region that was overlapped by the proximal interphalangeal joint region between the maximum extension, 50°, and maximum flexion positions in the LM radiographs. This finding suggests that the degree of superimposition of the proximal interphalangeal joint region on the navicular bone region in the solar projection scintigram will vary depending on the positioning of the distal limb.

The percentage overlap was the lowest in the maximum flexion position group. One third of the specimens showed no superimposition of the proximal interphalangeal joint on the navicular bone regions when they were positioned in maximum phalangeal flexion. Therefore, using this type of positioning in the solar projection scintigram should result in the least superimposition of the proximal interphalangeal joint on the navicular bone.

Recommendations regarding the solar projection scintigram can be made based on this study. The position of the navicular bone relative to the distal phalanx in a dorsal to palmar direction will not be affected by the angle of the pastern. Using a leg position where the sole of the foot is in complete contact with the face of the gamma camera and the phalanges are flexed as much as possible will result in solar projection images with the least superimposition of the proximal interphalangeal joint on the navicular region.

At the Division of Diagnostic Imaging clinic\* the solar projection scintigram is positioned by using the following technique (Figure 10). The horse should stand so its front feet are between 100 cm and 50 cm (depending on the size of the horse) from the gamma camera and it is facing the gantry. The gamma camera is positioned horizontally with the face of the camera 50-55cm above floor and facing up. A lexan shield is placed over the face of the gamma camera to protect it from being damaged by the horse's foot and a square piece of non-slip foam is put on this shield to prevent the horse's foot from slipping. The horse's front leg is lifted forward and up, and the sole of the foot is placed in the centre of the face of the gamma camera. The leg should be held around the fetlock joint and moderate pressure exerted on the dorsal aspect of the fetlock to; flex the phalanges, keep the sole flat on the face of the gamma camera, and hold the leg still for the acquisition of the image.

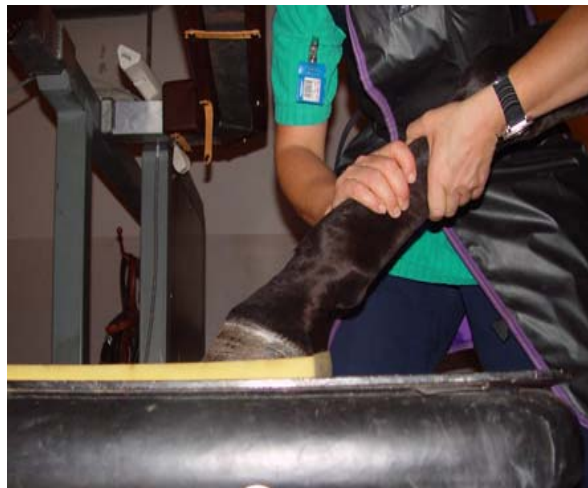


Figure 10. The positioning of a horses foot on the gamma camera for a solar projection scintigram. This position results in minimal superimposition of the PIPJ region on the navicular bone region.

We are currently developing a method using semi-automatic ROIs to locate the navicular bone region, based on the lateral width of the distal phalanx in the solar projection. The accuracy of ROI placement of this method will then be tested. If this method proves to be accurate then it will be possible to investigate the use of this objective measurement technique in the diagnosis of diseases of the navicular bone in horses.

## Conclusion

Information obtained from the radiographs in this study was used to develop a method to predict the position of the navicular bone in solar projection scintigrams. A technique for the solar projection that minimises superimposition of the proximal interphalangeal joint on the navicular bone is recommended.

## Acknowledgement

This study was supported by a grant from Stiftelsen Albert Hjärrefonden, Statens Veterinärmedicinska Anstalt, 751 89 Uppsala, Sweden.

## References

1. Keegan KG, Wilson DA, Lattimer JC, Twardock AR, Ellersieck MR. Scintigraphic evaluation of <sup>99m</sup>Tc-methylene diphosphate uptake in the navicular area of horses with lameness isolated to the foot by anaesthesia of the palmar digital nerves. *AJVR* 1996;57:415-421.
2. Steyn PF. Nuclear medicine. In: Stashak TS, ed. *Adams' Lameness in Horses*. Philadelphia, United States of America: Lippincott Williams and Wilkins; 2002:347-375.
3. Pilsworth RC, Dyson SJ. Practical scintigraphic examination of the horse. In: Dyson SJ, Pilsworth RC, Twardock AR, Martinelli MJ, eds. *Equine scintigraphy*. Newmarket, United Kingdom: Equine Veterinary Journal Ltd; 2003:75.
4. Ross MW, Stacy VS. Nuclear Medicine. In: Ross MW, Dyson SJ, eds. *Diagnosis and Management of Lameness in the Horse*. St Louis, United States of America: Saunders; 2003:198-212.
5. Pilsworth RC, Shepherd MC. Gamma Camera installations. In: Dyson SJ, Pilsworth RC, Twardock AR, Martinelli MJ, eds. *Equine scintigraphy*. Newmarket, United Kingdom: Equine Veterinary Journal Ltd; 2003:47-51.
6. Ueltschi G. Bone and joint imaging with <sup>99m</sup>Tc labelled phosphates as a new diagnostic aid in veterinary orthopaedics. *J Am Vet Radiol Soc* 1977;18:80-84.
7. Trout DR, Hornof WJ, O'Brien TR. Soft tissue- and bone-phase scintigraphy for diagnosis of navicular disease in horses. *JAVMA* 1991;1:73-77.
8. Turner TA. Differentiation of navicular region pain from other forms of palmar heel pain. *Pferdeheilkunde* 1996;12:603-606.
9. Ueltschi G. Stellenwert der Knochenszintigraphie und der Röntgenuntersuchung beim Problembereich der Podotrochlose. *Pferdeheilkunde* 1999;15:122-128.
10. Dyson S. Subjective and quantitative scintigraphic assessment of the equine foot and its relationship with foot pain. *Equine vet J* 2002;34:164-170.
11. Dyson S, Marks D. Foot pain and the elusive diagnosis. *Vet Clin Equine* 2003; 19:531-565.
12. Schwan M, Gerlach, Jahn W, Sill V. Quantitative assessment of nuclear bone scans using the regions of interest technique as applied to the navicular bone and insertion of the deep digital flexor tendon regions of interest in the distal phalanx of the horse. *EAVDI-12th annual conference 2005*. p41.

13. Devous MD, Twardock AR. Techniques and applications of nuclear medicine in the diagnosis of equine lameness. *JAVMA* 1984;184:318-325.

14. Erichsen C, Berger M, Eksell P. The scintigraphic anatomy of the equine sacroiliac joint. *Vet Radiol Ultrasound* 2002;43:287-292.

15. Twardock RA. Basic structure and function of the camera. In: Dyson SJ, Pilsworth RC, Twardock AR, Martinelli MJ, eds. *Equine scintigraphy*. Newmarket, United Kingdom: Equine Veterinary Journal Ltd; 2003:42.

16. Butler JA, Colles CM, Dyson SJ, Kold SE, Poulos PW. Fusion times of physes and suture lines. In: *Clinical Radiology of the Horse*. Oxford, United Kingdom: Blackwell Sciences; 2000:585-587.

\* Division of Diagnostic Imaging and Clinical Pathology,  
Department of Biomedical Sciences and Veterinary Public Health,  
Swedish University of Agricultural Sciences,  
Uppsala, Sweden.

† Siemens Optitop 150/40/80 HC-100L. Siemens AG, Munich, Germany.

‡ Siemens Polydoros Sx 80. Siemens AG, Munich, Germany.

§ Fuji IP Cassette type C with ST VI (LM radiographs) and HR-V (PrDi radiographs) imaging plates. Fuji Photo Film Co. Ltd. Japan.

|| Fujifilm FCR XG-1. Fuji Medical Imaging Co.Ltd. Japan.

¶ Centricity RA 600 V6.1 Diagnostik, GE Medical Systems, Slough, UK.

# Leukoplast, Beiersdorf AG, D-20245 Hamberg, Germany.

\*\*SigmaStat 3.0, Systat Software Inc., Richmond, California, USA.

## ACKNOWLEDGEMENTS

This study was carried out at the Division of Diagnostic Imaging and Clinical Pathology, Department of Biomedical Sciences and Veterinary Public Health, Faculty of Veterinary Medicine and Animal Science, Swedish University of Agricultural Sciences, Uppsala, Sweden.

Financial support was given by Stiftelsen Albert Hjärrefonden, Statens Veterinärmedicinska Anstalt, 751 89 Uppsala, Sweden.

My sincere thanks to:

My supervisor, Per Eksell. Your ability to organise discrete meetings with meat trucks in car parks in Uppsala will never be forgotten. Thank you for teaching me an enormous amount about scintigraphy, your wise advice, constant optimism and your bent sense of humour. I hope you will continue to be involved in some way with Diagnostic Imaging at SLU for many years to come.

Everyone in the Division of Diagnostic Imaging. You have all contributed in some way to this thesis and thank you for making this department a great place to work.

Peter Lord, Kerstin Hansson, Maggi Uhlhorn, and Estelle Ågren for being such good radiologists, teaching me so much about diagnostic imaging, and working for me in the clinic while I was away at courses. You have all created very positive and friendly learning environment and I am privileged to be working in this department with you all.

Ina Larsson, Mieth Berger, Vivan Eriksson and Lillan Löfrot for operating an excellent scintigraphy department, being enthusiastic about the project, phoning me every time a solar projection was about to be taken and posing for photos.

Lotte Erichsen, who originally started this project and gave me many ideas on how to continue it. Thank you for being enthusiastic, supportive, and generous with sharing your knowledge.

Martin Wierup and Bernt Jones for allowing me to do this degree whilst working in the department.

Marie Sundberg, for your unbelievable patience. I am sure there were many occasions when you had grave doubts about this study being completed and perhaps this is a record in the slowest printing of a thesis, but here it is finally!

Karin Östenson for directing the masters programme.

The Department of Pathology for collecting and storing the specimens that provided the material for this study.

Naruepon Kampa and Suwicha Chuthatep for your advice and interest and adding so much to the atmosphere of the department during your studies here.



All the masters students of 2004-5 Uranchimeg Tsegmed, Anas Al-Makhzoomi, Iftikhar Ali, Inoka Peiris and Pushkar Kulkarni. I wish you all the best for the future.

The majority of the work for this degree was done during family time. Thank you Timothy and Kristoffer for being such great children, and for putting up with me working late nights and weekends. Thank you Cecilia for everything, your love and taking me to see the world, for doing all the things that I didn't while I was doing this, reading endless manuscripts, correcting my English and keeping my life balanced and in perspective.



